



**HAL**  
open science

## Combining punctual and high frequency data for the spatiotemporal assessment of main geochemical processes and dissolved exports in an urban river catchment

Juan-Luis Lechuga-Crespo, Estilita Ruiz-Romera, Jean-Luc Probst, Jessica Unda-Calvo, Zaira Carolina Cuervo-Fuentes, Jose-Miguel Sanchez-Perez

### ► To cite this version:

Juan-Luis Lechuga-Crespo, Estilita Ruiz-Romera, Jean-Luc Probst, Jessica Unda-Calvo, Zaira Carolina Cuervo-Fuentes, et al.. Combining punctual and high frequency data for the spatiotemporal assessment of main geochemical processes and dissolved exports in an urban river catchment. *Science of the Total Environment*, 2020, 727, pp.138644. 10.1016/j.scitotenv.2020.138644 . hal-02896448

**HAL Id: hal-02896448**

**<https://hal.science/hal-02896448>**

Submitted on 10 Jul 2020

**HAL** is a multi-disciplinary open access archive for the deposit and dissemination of scientific research documents, whether they are published or not. The documents may come from teaching and research institutions in France or abroad, or from public or private research centers.

L'archive ouverte pluridisciplinaire **HAL**, est destinée au dépôt et à la diffusion de documents scientifiques de niveau recherche, publiés ou non, émanant des établissements d'enseignement et de recherche français ou étrangers, des laboratoires publics ou privés.



## Open Archive Toulouse Archive Ouverte

OATAO is an open access repository that collects the work of Toulouse researchers and makes it freely available over the web where possible

This is an author's version published in: <https://oatao.univ-toulouse.fr/26467>

### Official URL:

<https://doi.org/10.1016/j.scitotenv.2020.138644>

### To cite this version:

Lechuga-Crespo, Juan-Luis  and Ruiz-Romera, Estilita and Probst, Jean-Luc   
and Unda-Calvo, Jessica and Cuervo-Fuentes, Zaira Carolina and Sanchez-Pérez, José Miguel  *Combining punctual and high frequency data for the spatiotemporal assessment of main geochemical processes and dissolved exports in an urban river catchment.* (2020) *Science of the Total Environment*, 727. 1-19.  
ISSN 0048-9697 .

Any correspondence concerning this service should be sent to the repository administrator: [tech-oatao@listes-diff.inp-toulouse.fr](mailto:tech-oatao@listes-diff.inp-toulouse.fr)

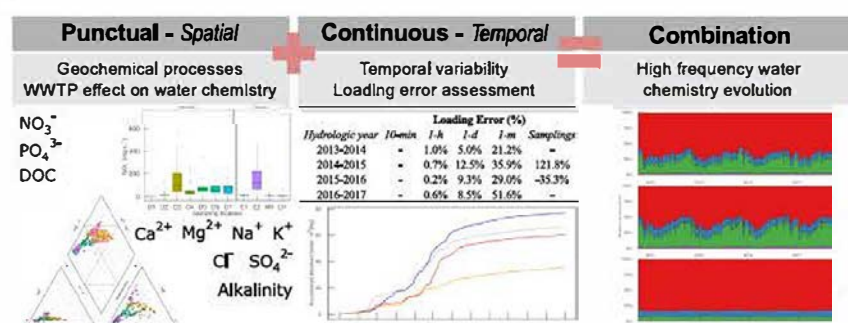
# Combining punctual and high frequency data for the spatiotemporal assessment of main geochemical processes and dissolved exports in an urban river catchment

Juan Luis Lechuga-Crespo<sup>a,b</sup>, Estilita Ruiz-Romera<sup>a,\*</sup>, Jean-Luc Probst<sup>b</sup>, Jessica Unda-Calvo<sup>a</sup>, Zaira Carolina Cuervo-Fuentes<sup>a</sup>, José Miguel Sánchez-Pérez<sup>b</sup>

<sup>a</sup> Department of Chemical and Environmental Engineering, University of the Basque Country, Plaza Ingeniero Torres Quevedo 1, Bilbao 48013, Basque Country, Spain

<sup>b</sup> ECOLAB, Université de Toulouse, CNRS, INPT, UPS, Campus ENSAT, Avenue de l'Agrobiopole, 31326 Castanet Tolosan Cedex, France

## GRAPHICAL ABSTRACT



## ABSTRACT

The assessment of dissolved loadings and the sources of these elements in urban catchments' rivers is usually measured by punctual sampling or through high frequency sensors. Nevertheless, the combination of both methodologies has been less common even though the information they give is complementary. Major ion ( $\text{Ca}^{2+}$ ,  $\text{Mg}^{2+}$ ,  $\text{Na}^+$ ,  $\text{K}^+$ ,  $\text{Cl}^-$ ,  $\text{SO}_4^{2-}$ , and alkalinity), organic matter (expressed as Dissolved Organic Carbon, DOC), and nutrients ( $\text{NO}_3^-$ , and  $\text{PO}_4^{3-}$ ) are punctually measured in the Deba river urban catchment (538 km<sup>2</sup>), in the northern part of the Iberian Peninsula (draining to the Bay of Biscay). Discharge, precipitation, and Electrical Conductivity (EC) are registered with a high frequency (10 min) in three gauging stations. The combination of both methodologies has allowed the assessment of major geochemical processes and the extent of impact of anthropogenic input on major composition of riverine water, as well as its spatial and temporal evolution. Three methodologies for loading estimation have been assessed and the error committed in the temporal aggregation is quantified. Results have shown that, even though carbonates dominate the draining area, the water major ion chemistry is governed by an evaporitic spring in the upper part of the catchment, while anthropogenic input is specially noted downstream of three wastewater treatment plants, in all nutrients and organic matter. The results of the present work illustrate how the combination of two monitoring methodologies allows for a better assessment of the spatial and temporal evolution on the major water quality in an urban catchment.

### Keywords:

Major ion  
Nutrients  
Environmental sensors  
Punctual sampling  
Method integration

\* Corresponding author.

E-mail addresses: juanluis.lechuga@ehu.eus (J.L. Lechuga-Crespo), estilita.ruiz@ehu.eus (E. Ruiz-Romera).

## 1. Introduction

Due to global population growth prospects in the following years (Ghanem, 2018), temporal and spatial assessments of anthropogenic influences on the ecosystem are of increasing interest. Among others, anthropogenic activity has influenced the delivery of elements (sediments, nutrients, organic matter, salts...) to streams both through point sources like facilities effluents, and diffuse sources like agriculture. Rivers act as a vector of transport for matter in the land to ocean continuum, though anthropogenic elements eventually arrive to coastal wetlands and the ocean, altering both freshwater and wetland ecosystems (Nielsen et al., 2003; Vörösmarty et al., 2010; Herbert et al., 2015). In the future, demographic growth is likely to keep on increasing human activities, and climate change is expected to alter hydrological regimes (Graham et al., 2007) causing moments of lower discharge, which would imply increases in dissolved solids concentration, threatening aquatic ecosystems (Vörösmarty et al., 2010; Cañedo Argüelles et al., 2013). Understanding the extents of such hazards' effect on ecosystem services and goods is needed to forecast potential consequences of these impacts, as well as evaluating the effects of management actions taken to reduce them (Cañedo Argüelles et al., 2013).

Focusing on the dissolved composition of water, the increase of dissolved inorganic solids ( $\text{Ca}^{2+}$ ,  $\text{Mg}^{2+}$ ,  $\text{Na}^+$ ,  $\text{K}^+$ ,  $\text{HCO}_3^-$ ,  $\text{CO}_3^{2-}$ ,  $\text{Cl}^-$ , and  $\text{SO}_4^{2-}$ ) concentration in streams is called salinization (Nielsen et al., 2003). Increases of ionic concentration caused by natural (primary salinization) or anthropogenic (secondary salinization) sources are potential hazards to freshwater environments (Kaushal et al., 2017). In the absence of anthropogenic influences, freshwater salinity originates from three sources: (1) weathering of the catchment, which is a function of both geology of the catchment and precipitation; (2) sea spray, although this is only important in coastal locations, and (3) wet deposition caused by the evaporation of seawater (Cañedo Argüelles et al., 2013). Organic matter and nutrients are commonly linked to the carbon, nitrogen, sulphur and phosphorus cycles, as complex interactions among biotic and abiotic elements in the riverine ecosystem are found (Anderson, 2016; Vitousek et al., 1997; Vitousek et al., 2009). When human inputs are present (through fertilization, wastewater effluents, road salt application...), increased dissolved loadings alter the natural cycles (Vitousek et al., 2009; Herbert et al., 2015). Usually, evaluations regarding dissolved solid loadings focus on agricultural catchments (e.g. Merchán et al., 2019, 2020; Vitousek et al., 2009) and less on urban environments (Khatri and Tyagi, 2015; Launay et al., 2016), where the saline input is in the form of point source. Commonly, the origin of these inputs are urban wastewater effluents (Álvarez Vázquez et al., 2016), systems where nutrients and turbidity are removed from water but where not act over major ion composition is taken unless tertiary treatment is present. In this sense, we ask the following question: which spatial and temporal influence have point sources on the streams?

To answer this question, a case study has been selected, and a monitoring program of the catchment has been established. Setting up a monitoring program within a system needs to capture the spatial and temporal variability of the processes given within a catchment and, with this purpose, punctual sampling campaigns are commonly taken with finer or lower temporal resolutions in the outlet, or spatially distributed in the catchment. Recently, the use of in situ sensors for the monitoring of water quality variables has become more common in these assessments (Rode et al., 2016), which allow for high frequency measurements performed in specific sites within a system (commonly a gauging station). However, such sensors are not capable of quantifying all variables that can be assessed within a laboratory, though each of these methodologies has present advantages and drawbacks for the assessment. Nevertheless, the combination of both punctual results and continuous registries poses an

opportunity to better understand the processes given and to assess their influences within a catchment as recently shown by Ponnou Delaffon et al. (2020), who highlighted nycthemeral cycles due to biological impact on nitrate concentrations and carbonate precipitation in streamwaters.

The urban catchment selected in this study is a medium size catchment where previous studies of surface water quality have identified physicochemical variables ( $\text{EC}$ ,  $\text{DOC}$ ,  $\text{PO}_4^{3-}$ ,  $\text{NO}_3^-$ ,  $\text{NO}_2^-$ ,  $\text{NH}_4^+$ ) and specific pollutants ( $\text{Cu}$ ,  $\text{Zn}$ ,  $\text{Pb}$ ,  $\text{Ni}$ ,  $\text{Cr}$ ) as main explainers of water pollution (Unda Calvo et al., 2020), however none of the previous studies has focused on the major ion composition, thus the study of major geochemical processes and the assessment of anthropogenic inputs on major chemistry remains unstudied. Both a monitoring program with punctual samplings and continuous registries are present in this catchment, posing an opportunity to evaluate the combination of both methodologies on the assessment of the anthropogenic impact on salinity.

Previous studies in the area (Ábalos et al., 2008; Iribar and Ábalos, 2011; Martínez Santos et al., 2015) have highlighted the geological structures and the effect they have on the water chemistry of this river. Saline springs are common in this area, as noted by Iribar and Ábalos (2011) and its influence on the Deba river catchment, found in the Lenitz Gatzaga area, has also been identified as relevant in the major ion composition of the water. Wastewater Treatment Plants (WWTP) effluents have also been found as major point sources of nutrients to the river streams, and the use of chemical compounds has been noted for phosphorus removal (Martínez Santos et al., 2018). However, the spatial and temporal extent of the WWTP effluents impact, and the influence of natural saline springs on water chemistry in this urban catchment have not been evaluated yet. Understanding the present state dynamics gives a starting point for forecasting studies. Other studies have shown that the Deba river catchment has a low capacity to absorb precipitation, making it vulnerable to extreme precipitation events, which are more likely to occur in climate change scenarios (Mendizabal et al., 2014). Considering hydrology as the main driver of suspended sediments (García García et al., 2019) and being sediments a vector of transport of pollutants (Unda Calvo et al., 2019a) in this catchment, the relevance of including the temporal analysis is justified. In this sense, the integration of punctual data from a monitoring program to the high frequency registries of the gauging stations in this catchment poses an opportunity on highlighting the hotspots and times regarding hazards to the water chemistry.

Then, for the assessment of geochemical and anthropogenic inputs into the Deba river urban catchment, we propose of the following hypothesis: a) the geochemical processes responsible of major ion characteristics of the Deba River are mainly affected by the head water southwestern part of the catchment due to the presence of a saline spring, and its influence is noted downstream to the outlet; and b) the urban and industrial treated and untreated waters have a greater impact in the middle part of the catchment, causing a shift in major ion composition and nutrients. In order to test these hypotheses, the aim of this study is to evaluate the dominant geochemical processes governing the major ion chemistry of the Deba river urban catchment, as well as assess the dissolved loadings to the estuary by combining punctual and continuous data. More specifically, the objectives of this study are: i) to identify the major geochemical processes controlling major ion chemistry along the main channel and tributaries, ii) to evaluate the possibilities of integrating punctual data on continuous registries for the estimation of dissolved loadings, iii) to assess the role of temporal resolution on the estimation of dissolved loadings. The results from this study are expected to improve the understanding of human impacts on urban environments with relevant geological influence, as well as to present a methodology for the integration of punctual samplings on continuous registries.

## 2. Materials and methods

### 2.1. Study area and sampling set up

The Deba catchment (538 km<sup>2</sup>) is located in the northern part of the Iberian Peninsula (West Europe), in the middle part of Donostia San Sebastian and Bilbao cities, mainly located in the Gipuzkoa province territory (Fig. 1). High slopes both in the hills and in the stream channel drain water to the Cantabrian Sea (part of the Atlantic Ocean) in the Bay of Biscay through a 62 km long river born in the southwest part of the catchment. Close to the Leintz Gatzaga saline springs, the Deba river receives the influent of the Mazmela tributary before flowing through the towns of Eskoriatza and Aretxabaleta and the city of Arrasate Mondragon, after which it receives the influent of the Oñati tributary to continue through Bergara city towards the lower part of the catchment, where the Ego tributary incorporates to the main channel before Elgoibar town and the villages of Alzola and Mendarozabal, reaching the ocean in the Deba city, which names both the river and the draining catchment. Within this hydrologic unit, there are other streams draining to the ocean which are not included in the present analysis, like the one outflowing in the city Mutriku.

Together with the cities, there are several industries in the area (Fig. 1b), which have made the Deba river the most polluted in the Gipuzkoa province (<https://www.gipuzkoa.eus/es/web/obrahidraulikoak>, accessed on November 2019). In the last years, the stakeholders have taken some management actions related to the treatment of the urban wastewaters, achieving a good ecological status in the last campaign of 2018 for most of the sampling locations, except for the lower part of the catchment and the lower part of the Ego tributary (URA, 2019). Among those actions, special mention is needed for the incorporation of three wastewater treatment plants (WWTP) between 2008 and 2012: the Epele WWTP in the southwest part of the catchment, before the confluence with the Oñati tributary; the Mekolalde WWTP, in the middle part of the catchment; and the Apraitz WWTP, in the lowest part of the catchment, after the incorporation of the Ego tributary (Fig. 1a, b).

The Epele WWTP collects the wastewaters from Eskoriatza, Aretxabaleta, Arrasate, and Oñati cities, treating an approximate load of 90,000 equivalent habitants; the Mekolalde WWTP takes the water from Bergara, and it is expected to be connected with Antzuola and other villages in the area, treating about 35,000 equivalent habitants; while the Apraitz WWTP treats the waters from Ermua, Eibar, and Elgoibar, the highest load of all the three (around 95,000 equivalent habitants) before draining the waters to the river. Both Epele and Mekolalde WWTP count with activated sludge and biological elimination of nitrogen but, while Epele WWTP uses biological elimination of phosphorus, Mekolalde WWTP uses a chemical procedure. In contrast, the Apraitz WWTP uses a sequential biological reactor (SBR), counting with biological elimination of nitrogen and chemical for phosphorus ([www.gipuzkoakour.eus](http://www.gipuzkoakour.eus)).

Before the set up of the WWTP, a monitoring program was established in the area with the installation of three gauging stations measuring a high frequency time series (every 10 min) variables such as accumulated precipitation, air and water temperature, discharge, electrical conductivity, among others. Registries have shown that, due to the latitude of the province and the placement in the Bay of Biscay, there is a high pluviometry (1384 mm·y<sup>-1</sup>) and a soft temperature (13 °C), with a seasonal distribution of the rainfall (<https://www.gipuzkoa.eus/es/web/obrahidraulikoak>, accessed on November 2019). This, together with the low ability of the Deba catchment system to infiltrate water (Mendizabal et al., 2014), causes periods with high discharge and very dry periods, yielding an annual average of 12.56 m<sup>3</sup>·s<sup>-1</sup> (<https://www.gipuzkoa.eus/es/web/obrahidraulikoak>, accessed on November 2019).

Even though the Deba river catchment has been noted as the most polluted in the area (Martínez Santos et al., 2015), most of the land is

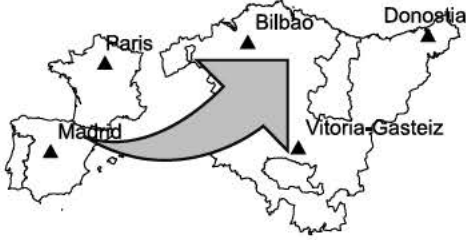
covered by forest or pasture (Fig. 1d), where only 2% of the territory is dedicated to agricultural purposes (according to the CORINE Land Cover database, 2012, available via the Copernicus Land Monitoring Service of the European Union). Though, most of the anthropogenic influence over the water quality and composition is expected to be related to the industrial and urban effluents from the WWTP and industries (Martínez Santos et al., 2015).

Due to the small distance from the coast, and the relatively homogeneous land use in contrast to the heterogeneous lithological groups in the area, the “natural” (not including the anthropogenic inputs) Deba river major ion composition is expected to be influenced mostly by geochemical processes related to water rock interaction, i.e. chemical weathering. Regarding the geological context, this catchment is located between the Bilbao Anticlinorium and the Biscay Sinclinorium, with rock ages varying from the Aptian Albian to the Paleogene (Iribar and Ábalos, 2011). Within the Bilbao Anticlinorium area, which is located in the upper and middle part of the catchment, there are some thrust faults and secondary faults showing Cenomanian Aastrichtian, Albian, Aptian Albian, and Kimmeridgian Barremian layers (Iribar and Ábalos, 2011, EVE, 1989). Scattered around this southwestern part of the catchment, there are several saline water springs, gypsum and evaporites sites (Fig. 1b) related to Walden Facies, which are expected to have an effect on the major ion composition of the groundwater and surface water in the Deba river catchment. It is important to note that the official lithological map lacks the representation of these gypsum and evaporitic sites.

Regarding the geochemistry of the underlying rocks, the Deba catchment area is dominated by detritic rocks, mixed with alternate marls and clays, presenting different lithological configurations for three sections: the southwest part (draining to San Prudentzio gauging station, Fig. 1b); the southeast part (draining to Oñati gauging station, Fig. 1b), and the Ego tributary in the middle west part of the catchment. The southwest part presents slates and is the most related to the saline springs and gypsum sites (Iribar and Ábalos, 2011), the southeast part drains mainly detritic rocks, while the Ego tributary is mainly conformed by limestones. The mid lower part of the catchment presents a stripe with volcanic rocks.

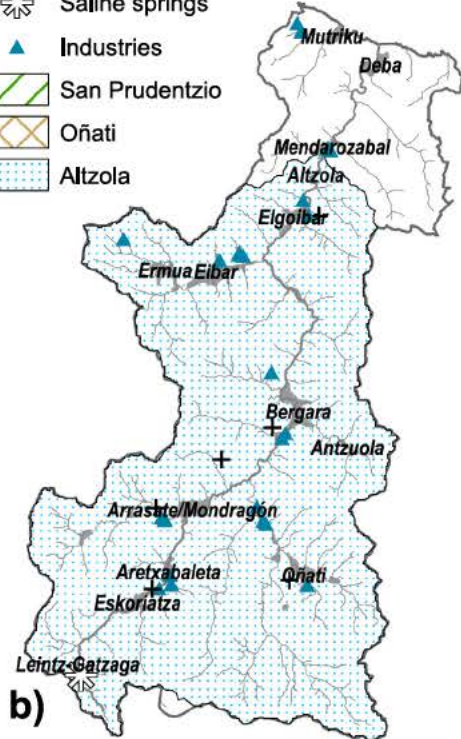
### 2.2. Field and laboratory methods

In order to control the major chemical composition of the catchment, and assess the potential anthropogenic effect, a set of 11 sampling locations has been established and sampled along the main channel and tributaries, since April 2014 to January 2017. The location of the sampling spots is shown in Fig. 1: along the main channel, D1 was considered as the control area associated with low human impact, this sampling location is placed before the input of any spring and drains 6.2 km<sup>2</sup>. The Deba river flows downstream until it receives the waters from the Mazmela tributary, where a sampling location is also present, M1 (3.5 km<sup>2</sup>). After Eskoriatza and Aretxabaleta, the sampling location D2 is placed in the main channel (62.4 km<sup>2</sup>, accumulated area), before the river crosses Arrasate Mondragon. Before the river gets to the confluence with Oñati (where one sampling location is placed: O1, 130 km<sup>2</sup>), other sampling location is established, D3 (121 km<sup>2</sup>). After the confluence, D4 (321 km<sup>2</sup>) and D5 (329 km<sup>2</sup>) are closely placed, before the river changes its course towards the northwest to meet the Ego tributary confluence. In the Ego tributary, due to its polluted characteristics, two sampling locations are placed, E1 in the upper part of the catchment (2.4 km<sup>2</sup>), and E2 before the confluence with the main channel (55.5 km<sup>2</sup>). After the confluence, the D6 sampling location collects the mixed water (419 km<sup>2</sup>) now directed to the northeast part, where D7 is placed close to the transition zone of the river to the ocean (486 km<sup>2</sup>). From the anthropogenic influence assessment point of view, there are four sampling locations with special interest: D3 receives the influence of the Epele WWTP, D5 registries the Mekolalde

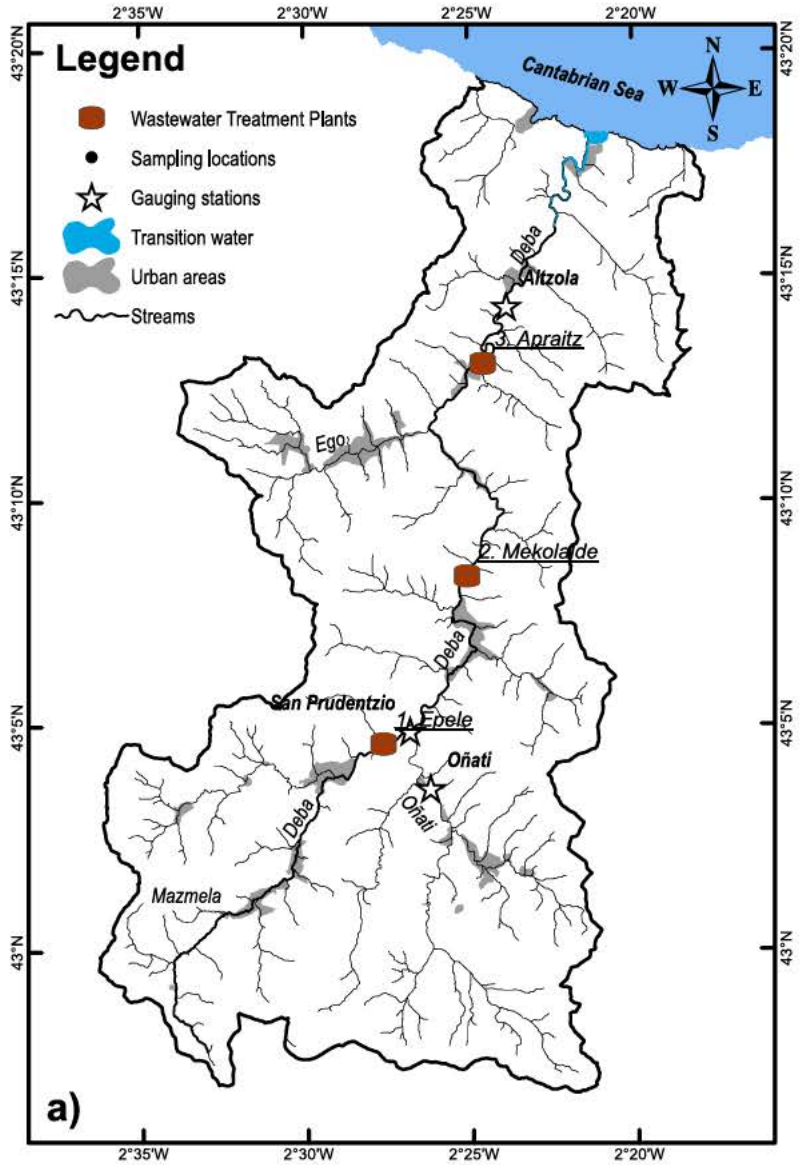


### Legend

- + Urban waste deposits
- ☼ Saline springs
- ▲ Industries
- ▨ San Prudentzio
- ▨ Oñati
- ▨ Altzola

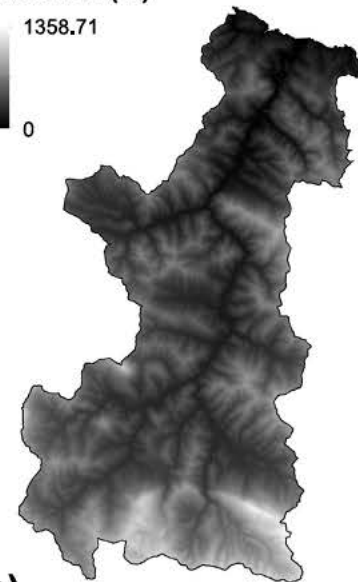
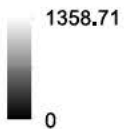


b)



a)

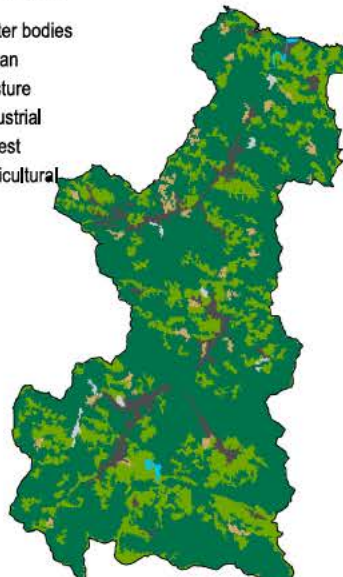
### Elevation (m)



c)

### Land Use

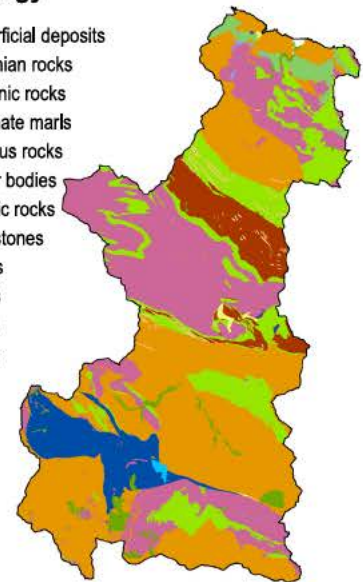
- Water bodies
- Urban
- Pasture
- Industrial
- Forest
- Agricultural



d)

### Lithology

- Superficial deposits
- Philonian rocks
- Volcanic rocks
- Alternate marls
- Igneous rocks
- Water bodies
- Detritic rocks
- Limestones
- Slates
- Ofites
- Marls
- Clays



f)

**Table 1**

Summary of physicochemical characteristics for each sampling location in the main channel and tributaries. Values are presented as mean, minimum (Min) and maximum (Max) for each place. The number of samples for each variable is represented by n, when some values were missing, superscripts were added in the mean cell (<sup>a</sup> means 1 missing value, <sup>b</sup> represents 2, and <sup>c</sup> represents 3). Measured variables are pH (unitless), Alkalinity (meq·L<sup>-1</sup>), Electrical Conductivity in field (EC<sub>field</sub>, µS·cm<sup>-1</sup>), Total Dissolved Solids in field (TDS<sub>field</sub>, mg·L<sup>-1</sup>), organic matter expressed as Dissolved Organic Carbon (DOC, mg·L<sup>-1</sup>), nutrients concentrations including NO<sub>3</sub><sup>-</sup> and P-PO<sub>4</sub><sup>3-</sup>, as well as major anions (Cl<sup>-</sup>, SO<sub>4</sub><sup>2-</sup>) and cations (Ca<sup>2+</sup>, Mg<sup>2+</sup>, Na<sup>+</sup>, and K<sup>+</sup>) concentrations (mg·L<sup>-1</sup>).

Sampling location		pH	Alkalinity	EC <sub>field</sub>	TDS <sub>field</sub>	DOC	NO <sub>3</sub>	P-PO <sub>4</sub> <sup>3-</sup>	Cl	SO <sub>4</sub> <sup>2-</sup>	Ca <sup>2+</sup>	Mg <sup>2+</sup>	Na <sup>+</sup>	K <sup>+</sup>
Main channel														
D1 n = 11	Mean	7.9	1.8	474.6	281.2 <sup>b</sup>	1.8	1.1	2.1	67.1	35.3	43.8 <sup>a</sup>	6.0 <sup>a</sup>	35.6 <sup>a</sup>	1.5 <sup>a</sup>
	Min	7.5	1.1	203.4	110.8	0.2	0.6	0.9	17.3	15.4	22.7	3.0	9.1	0.9
	Max	8.2	3.0	1153.0	622.8	3.9	2.6	4.1	190.2	84.5	83.2	12.1	93.9	3.6
D2 n = 23	Mean	8.2	2.9	1050.9	569.2 <sup>b</sup>	3.6	2.0	20.0 <sup>a</sup>	151.9	148.4	97.7 <sup>a</sup>	14.1 <sup>a</sup>	86.6 <sup>a</sup>	4.2 <sup>a</sup>
	Min	7.5	1.5	343.5	182.9	0.6	0.3	3.1	14.7	57.9	44.1	5.7	9.5	1.3
	Max	8.9	3.8	2015.0	1090.0	5.8	5.1	118.3	379.7	223.3	138.6	20.8	217.4	11.3
D3 n = 24	Mean	8.1	2.7	716.3	386.5 <sup>b</sup>	4.1	7.4	168.2 <sup>a</sup>	74.5	104.9	80.2 <sup>a</sup>	9.6 <sup>a</sup>	43.5 <sup>a</sup>	5.9 <sup>a</sup>
	Min	7.1	1.7	330.1	176.0	0.4	1.0	6.0	12.8	48.4	45.4	4.9	8.2	1.2
	Max	8.8	3.6	1123.0	607.3	6.8	23.7	694.4	158.9	138.0	103.0	13.1	86.8	15.1
D4 n = 23	Mean	8.1	2.6	462.3	250.7 <sup>b</sup>	3.2	4.2	58.8 <sup>a</sup>	33.8	50.9	60.7 <sup>a</sup>	5.7 <sup>a</sup>	21.0 <sup>a</sup>	2.9 <sup>a</sup>
	Min	7.2	1.6	288.6	152.6	0.7	1.4	7.2	9.3	23.5	37.6	3.1	5.7	1.0
	Max	8.8	4.2	712.3	382.3	5.1	9.3	250.4	90.7	86.4	83.6	8.3	67.0	7.2
D5 n = 12	Mean	8.3	2.5	430.4	242.0 <sup>c</sup>	3.0	5.8	88.9 <sup>a</sup>	29.6	51.1	60.0 <sup>a</sup>	5.5 <sup>a</sup>	18.1 <sup>a</sup>	2.8 <sup>a</sup>
	Min	7.8	2.1	291.6	159.2	0.1	1.6	17.2	10.5	30.3	46.1	3.9	7.2	1.4
	Max	8.9	3.1	651.7	349.9	5.3	11.2	346.4	73.8	74.8	76.3	7.4	41.2	6.8
D6 n = 23	Mean	8.1	2.6	427.3	230.1 <sup>b</sup>	3.5	4.5	67.3 <sup>a</sup>	28.4	40.3	59.2 <sup>a</sup>	5.0 <sup>a</sup>	17.5 <sup>a</sup>	2.9 <sup>a</sup>
	Min	7.3	1.7	286.7	152.4	1.1	1.3	14.7	9.5	20.0	38.7	2.9	6.0	1.0
	Max	8.6	3.3	689.6	355.5	6.4	9.1	216.8	69.5	67.6	79.1	7.3	37.9	7.1
D7 n = 11	Mean	8.1	2.5	407.3	226.3 <sup>b</sup>	3.5	6.6	85.7	28.0	41.7	57.4 <sup>a</sup>	4.9 <sup>a</sup>	16.9 <sup>a</sup>	3.1 <sup>a</sup>
	Min	7.6	2.2	298.1	162.7	0.4	2.0	21.9	12.1	26.3	49.8	4.1	9.2	1.5
	Max	8.6	3.0	586.8	314.4	6.6	11.4	247.3	59.9	59.5	73.0	5.9	36.8	7.0
Tributaries														
M1 n = 23	Mean	7.9	3.2	777.4	402.7 <sup>b</sup>	2.7	1.7	7.8 <sup>a</sup>	30.1	207.2	101.8 <sup>a</sup>	20.2 <sup>a</sup>	33.2 <sup>a</sup>	3.9 <sup>a</sup>
	Min	7.4	1.0	330.5	173.7	0.8	0.2	0.1	14.8	60.6	35.6	6.1	12.8	1.5
	Max	8.5	5.2	1250.3	556.6	5.5	5.2	31.9	48.5	451.0	151.6	33.2	62.9	8.0
O1 n = 23	Mean	8.1	2.1	259.2	139.6 <sup>b</sup>	2.4	1.8	8.8 <sup>a</sup>	6.1	15.5	44.2 <sup>a</sup>	2.8 <sup>a</sup>	4.3 <sup>a</sup>	1.1 <sup>a</sup>
	Min	7.2	1.4	185.9	98.9	0.6	0.3	0.4	3.5	7.7	30.3	1.7	2.2	0.7
	Max	8.7	2.8	356.4	184.5	5.2	4.5	58.9	9.2	30.3	59.0	4.4	7.3	2.2
E1 n = 19	Mean	8.1	3.8	417.0	222.0 <sup>b</sup>	3.0	1.7	12.3	11.1	13.1	73.4	5.0	6.6	1.3
	Min	7.7	2.0	266.8	142.0	0.4	0.3	1.7	8.0	7.0	38.7	2.4	3.3	1.0
	Max	8.6	4.7	488.4	252.9	6.2	6.6	27.1	14.1	18.5	87.3	6.0	10.9	2.7
E2 n = 23	Mean	8.0	3.5	432.8	230.6 <sup>b</sup>	4.5	5.7	167.0 <sup>a</sup>	17.8	17.8	70.2 <sup>a</sup>	3.7 <sup>a</sup>	10.4 <sup>a</sup>	2.7 <sup>a</sup>
	Min	7.6	2.5	323.0	169.9	0.4	1.3	30.0	10.1	11.1	52.0	2.1	4.8	1.1
	Max	8.6	4.2	542.1	285.5	7.2	10.0	431.6	32.0	27.3	80.0	5.7	22.1	5.6

WWTP effect, E2 accounts for the Ermua and Eibar influence, and the D7 covers the Apraitz WWTP impact.

Every sampling location was sampled monthly or bimonthly between April 2014 and January 2017, covering two full hydrological years: 2014–2015 and 2015–2016, both beginning in October 1st, and part of the 2013–2014 and 2016–2017 hydrological years. All eleven sampling locations were sampled within a day, where waters were taken from the middle part of the river in 1 L pre-cleaned polyethylene bottles which were later taken at 4 °C to the laboratory in the Chemical and Environmental Engineering department of the University of the Basque Country (UPV/EHU), to be analyzed. In addition to the water sample, a Crison EC Meter Basic 30+, and a Crison Micro pH 2000 sonde were used to measure in situ Electrical Conductivity (EC), Total Dissolved Solids (TDS), and pH, respectively.

Once in the laboratory, samples were filtered through 0.45 µm filters to separate the suspended particles from the dissolved phase. One replicate of the filtered sample was acidified to 0.2% with HNO<sub>3</sub><sup>-</sup> (68%) for base cations (Ca<sup>2+</sup>, Mg<sup>2+</sup>, Na<sup>+</sup>, and K<sup>+</sup>) analysis using ICP OES (Perkin Elmer Optima 2000). One replicated of the filtered sample (non acidified) was used to analyze (Cl<sup>-</sup>, NO<sub>3</sub><sup>-</sup>, and SO<sub>4</sub><sup>2-</sup>) using ion chromatography (DIONEX ICS 3000). Alkalinity was determined using a Total Organic Carbon Analyzer (TOC L Shimadzu). Due to the pH ranges, the alkalinity values were converted to HCO<sub>3</sub><sup>-</sup> concentration in (mg·L<sup>-1</sup>).

Sample analysis was validated by computing the Ionic Charge Balance (ICB) between anions and cations for each sample following  $ICB = \frac{([Z^+] - [Z^-])}{([Z^+] + [Z^-])}$ , where [Z<sup>+</sup>] and [Z<sup>-</sup>] represents the sum of all cation and all anion concentrations expressed in meq·L<sup>-1</sup>. Samples showing |ICB| > 10% were discarded from the analysis. A summary of all the results of these analyses is shown in Table 1.

In addition to the punctual sampling methodology, three gauging stations measure hydrological (precipitation, discharge) and quality (turbidity, suspended sediment concentration, EC) variables at a 10 min frequency. EC is measured through in flowing water pumped to the station from the river. The three gauging stations are San Prudentzio and Oñati in the upper part of the catchment, and Altzola near the outlet (Fig. 1a, b). The Altzola gauging station, placed between D6 and D7 sampling locations in the lower part of the catchment, collects 464.25 km<sup>2</sup> of the area of the basin according to [www.geoesukadi.eus](http://www.geoesukadi.eus). Within this drainage area, San Prudentzio (121.78 km<sup>2</sup>) and Oñati (105.78 km<sup>2</sup>) are located close to D3 and O1 sampling locations, respectively, collecting independent draining surfaces. There is a relevant tributary in terms of discharge and chemical compounds which is not controlled by a gauging station: the Ego tributary in the western part of the catchment. At this moment, the contribution of this stream to the main channel may only be estimated qualitatively through the analysis of the chemical analysis carried in the monitoring program or through

**Fig. 1.** Study area localization and description: a) catchment extent and borders, together with main channel and tributaries, sampling locations, urban areas, wastewater treatment plants, and gauging stations; b) main human settlements, with principal industries, urban waste deposits, saline springs and main subasins, shaded for each gauging station; c) digital elevation model (DEM) showing orography; d) lithological groups derived from official maps; e) soil types according to FAO classification (FAO et al., 2012); and f) relevant land uses derived from the CORINE Land Cover map (EEA, 2012).

modelling, but hydrological modelling has not been performed for the present study.

### 2.3. Statistical analysis

All statistical analysis performed in the present study has been accomplished using R software (R Core Team, 2019) for handling the data. Four sections may be described for the data analysis followed: punctual data, regarding the study of the monitoring program results; continuous data, regarding the analysis of the gauging station registries; the punctual and continuous data integration, regarding the combination of the two sources of data; and the analysis of flood events.

#### 2.3.1. Analysis of the punctual data

Once the water samples were brought to the laboratory, the results of the analysis were compiled in a database. Graphs including the Gibbs plot, Piper diagram, and ionic ratios were constructed using the “ggplot2” library (Wickham, 2016). Due to the non normality, the data base was log transformed to reduce skewness before a correlation matrix was performed to see which variables were independent. Later, a Principal Component Analysis (PCA) with a Varimax rotation of the factors was used to reduce the number of variables, in order to distinguish the geochemical groups and the anthropogenic influence in the sampling locations for the different sampling periods. Finally, a Cluster Analysis (CA) was also performed using Euclidean square distance and the Ward's aggregation method to evaluate the degree of similitude among sampling locations for the three sampling periods.

#### 2.3.2. Analysis of the continuous data

From the three gauging stations registries, accumulated precipitation (mm), average discharge ( $\text{m}^3 \cdot \text{s}^{-1}$ ), water temperature ( $^{\circ}\text{C}$ ), pH (dimensionless), and average EC ( $\mu\text{S} \cdot \text{cm}^{-1}$ ) were selected for further analysis. For the Altzola gauging station, the start of the time series is in 1995 (July the 12th), for the San Prudentzio is in 1996 (July the 9th), and for the Oñati is in 1995 (April the 19th). The time series were validated by erasing negative values of accumulated precipitation, discharge, pH, and EC, introducing missing values in the analysis. Then, the 10 min registries were time aggregated to hourly by summing the accumulated precipitation and computing the arithmetic mean for discharge, temperature, pH, and EC. The hourly time series was then further aggregated to daily, monthly and yearly, following the same criteria.

#### 2.3.3. Punctual and continuous data integration

Punctual data were integrated using the daily aggregated time series and considering the punctual sample as representative for the day of the sampling campaign. EC and major ion concentrations in D6, D3, and O1 were incorporated to the Altzola, San Prudentzio, and Oñati time series, respectively. The gauging station and field EC were compared by means of the Pearson correlation finding a strong and significant correlation ( $r > 0.9$ ,  $p < 0.01$ ), and the correlation between  $\text{TDS}_{\text{field}}$  and  $\text{EC}_{\text{field}}$  is also strong and significant ( $r > 0.99$ ,  $p < 0.01$ ), while the extrapolation of TDS and major ion composition to a continuous time series was performed by computing a regression between the laboratory ionic concentration vs the  $\text{EC}_{\text{field}}$ . Three kinds of regressions are included: linear, potential, and logarithmic. Estimates of the parameters are calculated using the “stats” package in R for linear regression, and “minpack.lm” package (Elzhov et al., 2016) for non linear fit. Prediction intervals (PI, 95%) have been calculated checking normality within the samples of each sampling location through a Shapiro Wilk test ( $p < 0.01$  imply the rejection of the null hypothesis, data non normally distributed). Non linear fit has been accomplished by Levenberg Marquardt algorithm, and PI are calculated using uncertainty propagation through Taylor expansion and Monte Carlo simulation ( $n = 10^6$  simulations) contained in the “propagate” package (Spiess, 2018). Then, continuous

registries from EC were used as a proxy for the continuous concentration calculation.

## 3. Results and discussion

### 3.1. Sampling campaigns' results

#### 3.1.1. Overview

A summary of the results from the punctual monitoring campaigns is shown in Table 1. In general, the pH ranges from 7.1 (D3) to 8.9 (D5) yielding neutral to slightly alkaline characteristics to the waters in all the system, relevant changes are not found nor in the main channel or the tributaries, nor within sampling campaigns in each location. In contrast, the highest mean values for alkalinity are found in the Ego tributary, while the lowest in the upper part of the catchment (D1), finding all values between 1.1 and  $5.2 \text{ meq} \cdot \text{L}^{-1}$ . EC spans over an order of magnitude from  $185.9 \text{ (O1)}$  to  $2015.0 \mu\text{S} \cdot \text{cm}^{-1}$  (D2), reaching a mean peak ( $1050.9 \mu\text{S} \cdot \text{cm}^{-1}$ ) in the southwest part of the catchment (D2) decreasing towards the outlet, being the waters from Oñati (O1) the most diluted (mean  $259.2 \mu\text{S} \cdot \text{cm}^{-1}$ ). Similar trends are found for TDS, where headwater sampling locations on the southwest part of the catchment (D1, and M1) present a wider difference between minimum and maximum TDS concentration, in comparison with the other upper sampling locations, O1 and E1.

Regarding major ions at the catchment level, the cationic mean concentration predominance is  $\text{Ca}^{2+} > \text{Na}^{+} > \text{Mg}^{2+} > \text{K}^{+}$ , but their relative contribution to the TDS is different among ions: one group ( $\text{Ca}^{2+}$ ,  $\text{Mg}^{2+}$ , and  $\text{Na}^{+}$ ) present the greatest concentration in D2, as occurred for EC and alkalinity, but  $\text{K}^{+}$  concentration evolves similarly to nutrients and organic matter, peaking in D3.  $\text{Na}^{+}$  presents the highest differences between minimum and maximum concentration in D2, spanning over two orders of magnitude, while in other sampling locations this range is lower. Similarly happens with major anions ( $\text{Cl}^{-}$  and  $\text{SO}_4^{2-}$ ) for which peak concentrations are found in D2, but their spatial evolution is slightly different:  $\text{Cl}^{-}$  concentration decrease from D2 downstream, while  $\text{SO}_4^{2-}$  presents slightly increasing trends between D1 D2, D4 D5, and D6 D7.

Concerning dissolved organic carbon (DOC) and nutrients ( $\text{NO}_3^{-}$  and  $\text{P PO}_4^{3-}$ ) along the main channel, the lowest concentration are in the D1 sampling location, while the highest concentrations are found at D3, both in the southwest part of the catchment before the confluence of the Oñati stream. Relative to their own ranges,  $\text{P PO}_4^{3-}$  presents the widest differences between low and high concentration, specially at D3, as well as the greatest heterogeneity in extreme values among sampling spots, as shown in the Ego tributary, where the greatest concentration is found for E2 and it is around 20 times the highest concentration upstream, in E1.

Further punctual analysis has been taken in the present system, focusing on the metallic pollution both in water and sediments (Martínez Santos et al., 2015; Unda Calvo et al., 2017, 2019a, 2020). Those studies have shown and assessed the influence of anthropogenic inputs in the waters and sediments within this catchment focusing on metallic pollution, however the assessment of whether these human activities affect the major ion composition of water is remaining. Martínez Santos et al. (2015) suggested that partially treated or untreated wastewater effluents are the main source of organic matter in some specific sites of the catchment. Their study was based on the samples taken in 2011 and 2012, at the time when management actions were put in place, such as the commissioning of three wastewater treatment plants (WWTP, Fig. 1). In the present analysis, samples taken after the installation of these WWTPs are considered, and still different spatial and temporal patterns between saline concentrations and organic matter (in the form of DOC) and nutrients concentrations in the catchment are present. Further analysis is presented in Sections 3.1.2 and 3.1.4 regarding these spatial and temporal patterns.

### 3.1.2. Spatial evolution

The waters in the Deba river catchment are mixed along the main channel, receiving inputs from several tributaries (specially the Mazmela, Oñati, and Ego). Concerning TDS (Fig. 2a) and saline concentrations (Fig. 2b), the highest values for major ion concentrations are in D2, showing a decreasing trend towards the outlet of the catchment. In opposition, DOC, P,  $\text{PO}_4^{3-}$ , and  $\text{NO}_3^-$  peak in D3 (Fig. 2a) and show increasing trends between D4, D5 and D6, D7. Among the tributaries, and paying special attention to the sampling locations close to the main stream (M1, O1, and E2), three different aspects are relevant: Mazmela (M1) presents the highest concentrations for  $\text{Ca}^{2+}$ ,  $\text{Mg}^{2+}$ , and  $\text{SO}_4^{2-}$  in all the system, Oñati (O1) has the lowest saline concentrations, and the Ego tributary (E2) inputs a relevant amount of DOC, P,  $\text{PO}_4^{3-}$ , and  $\text{NO}_3^-$ . Previous studies in the area (Martínez Santos et al., 2018; Unda Calvo et al., 2020) have attributed the highest water quality index to all headwater sampling locations (D1, M1, O1, and E1) and the

lowest to (D3, D5, and D7) suggesting that the later group is influenced by effluents from wastewater treatment plants (WWTPs) and untreated urban wastewater (UWW), this is shown in the increasing trends between D2, D3, D4, D5, and D6, D7 in organic matter (DOC) and nutrients ( $\text{PO}_4^{3-}$ , and  $\text{NO}_3^-$ ). Other study (Iribar and Ábalos, 2011) has reported the influence of spring waters in the composition of river chemistry in this and surrounding catchments, and the presence of a saline spring in Leintz Gatzaga (between D1 and D2, Fig. 1b) seems to be responsible of the peak in saline concentration in D2 which is later noted down stream at the outlet. This is particularly important for  $\text{Na}^+$  and  $\text{Cl}^-$ , which are the main ions drained by this evaporitic spring (Ábalos et al., 2008), and for  $\text{SO}_4^{2-}$ , which is mainly associated to gypsum intrusion deposits in the Walden Facies in the Mazmela subasin (M1) (Ábalos et al., 2008; Iribar and Ábalos, 2011; Martínez Santos et al., 2015). D2 presents the highest saline concentration, reaching the oligohaline threshold ( $0.5 \text{ mg} \cdot \text{L}^{-1}$ ), which is later diluted till reaching

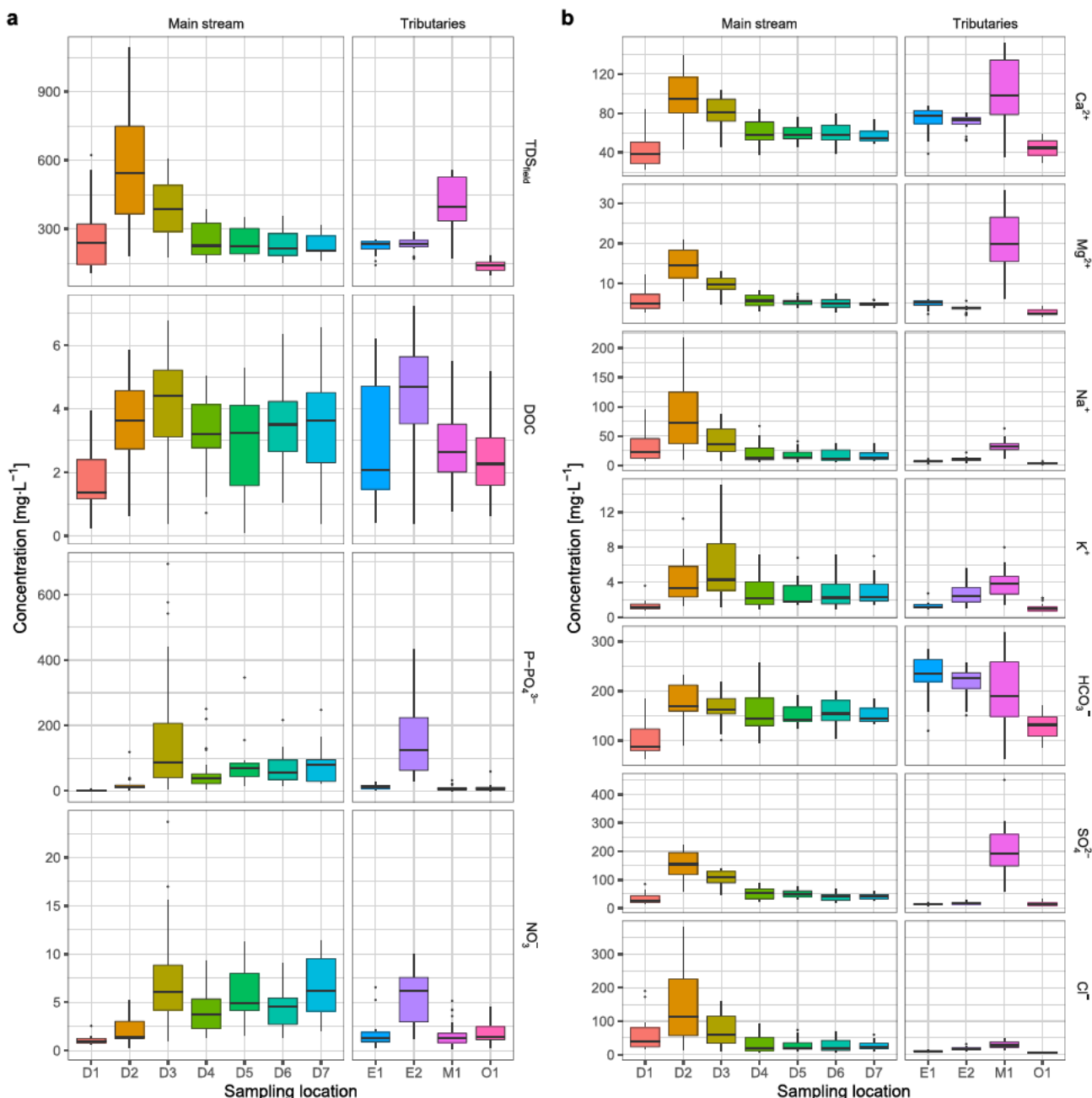


Fig. 2. Boxplot spatial evolution for a) TDS, DOC, and nutrients, and b) major ion composition, expressed as concentration ( $\text{mg} \cdot \text{L}^{-1}$ ). Two groups are present: main channel and tributaries.

freshwater characteristics in the mid and lower part of the catchment, suggesting that the saline spring is the dominant factor on the saline composition and that downstream sampling locations are dilution water.

### 3.1.3. Sampling campaign classification

Each punctual sampling campaign was performed within a day for all sampling locations, and the results are considered as representative of that day, without taking in consideration diurnal cycles or sub daily sampling, this assumption is later discussed in Section 3.2. Due to the differences found between the minimum and maximum values for each variable in each sampling location, a temporal assessment was considered necessary to understand the evolution of geochemical and WWTP influence on the water chemistry. In order to perform such assessment, a classification of the sampling campaigns regarding hydrological periods was included. This classification has been based on the daily mean discharge in the Altzola gauging station, and its relative value with regards to the 1st and 3rd quartiles of the October 2013 to September 2017 discharge time series. When the daily mean discharge was under the 1st quartile (P25th percentile,  $1.8 \text{ m}^3 \cdot \text{s}^{-1}$ ) the sampling campaign was classified as “low discharge” period, when it was over the 3rd quartile (P75th percentile,  $8.9 \text{ m}^3 \cdot \text{s}^{-1}$ ) it was attributed to “high discharge”, and all other samples between were classified as “mid discharge”. A potential source of uncertainty in this classification is not considering whether the sampling campaign was performed at the beginning or ending of a flood event, which is likely to condition the assessment of water and dissolved solid transports. These processes are taken in consideration and discussed in further sections (Section 3.2). Nevertheless, precipitation and discharge between Altzola San Prudentzio, and Altzola Oñati show a strong and significant correlation ( $r^2 > 0.8$ ,  $p < 0.01$ ) suggesting that, even though event characteristics are not considered, the dilution processes are expected to be uniform in all sampling stations, supporting the classification scheme. The Altzola discharge time series and the sampling classification is shown in Fig. 3.

### 3.1.4. Temporal evolution

Sampling periods (low, mid, and high discharge) were compared among them, to test whether the catchment response was homogeneous under different hydrological conditions or there was some

variation along time. Such comparison was performed making a Cluster Analysis (CA) on the sampling locations. Differences in the aggregation groups would indicate where and when there is a geochemical or an anthropogenic influence on the water chemistry. Before performing a CA, a Shapiro Wilk test for each of the variables has showed significant  $p$  value ( $p < 0.01$ ) for every variable, allowing the rejection of the null hypothesis of normal distribution of the variable, thus all variables are non normally distributed. In light of the distribution, considering that all variables are continuous and positive and that the numeric ranges are dislike among variables, a log transformation is applied before performing any other test. From the Pearson correlation matrix (Table 2) performed to the log transformed punctual dataset, a set of 10 variables (pH,  $\text{TDS}_{\text{field}}$ ,  $\text{EC}_{\text{field}}$ ,  $\text{Ca}^{2+}$ ,  $\text{Mg}^{2+}$ ,  $\text{Na}^+$ , Alkalinity,  $\text{SO}_4^{2-}$ ,  $\text{Cl}^-$ ,  $\text{P}$ ,  $\text{PO}_4^{3-}$ ) which were, at least, non correlated to one of the other variables were added to the CA. pH presents a non significant ( $p > 0.05$ ) to very significant ( $p < 0.01$ ) but low correlation ( $|r| < 0.25$ ) to all variables, which in conjunction with the low variation in this variable suggests low influence of acidic inputs in this catchment. In contrast,  $\text{TDS}_{\text{field}}$  and  $\text{EC}_{\text{field}}$  present a very significant and perfect positive correlation ( $r = 1$ ) among them, and a very strong correlation to all major cations ( $\text{Ca}^{2+}$ ,  $\text{Mg}^{2+}$ ,  $\text{Na}^+$ , and  $\text{K}^+$ ), supporting the findings on main influence of saline concentrations on the TDS found in the catchment.  $\text{Ca}^{2+}$  presents very significant but lower correlation to  $\text{Na}^+$  and  $\text{K}^+$  ( $0.7 < r < 0.74$ ), indicating a different behavior among these ions, which is also present on the relation of Alkalinity to all other variables, except for  $\text{Ca}^{2+}$  where the correlation is higher ( $r > 0.8$ ). Almost perfect fit is found between  $\text{Na}^+$  and  $\text{Cl}^-$  indicating a common origin in the catchment, which also present the highest correlation with  $\text{EC}_{\text{field}}$ , suggesting that among the saline concentrations in this catchment  $\text{Na}^+$  and  $\text{Cl}^-$  have the greatest influence on the  $\text{EC}_{\text{field}}$  and  $\text{TDS}_{\text{field}}$ . Among the organic matter and nutrients, there is a very significant correlation with  $\text{K}^+$ , but not a very strong correlation ( $r < 0.5$ ), which in contrast is found for  $\text{NO}_3^-$  and  $\text{PO}_4^{3-}$ .

Three dendrograms are shown in Fig. 4 for each sampling periods. Within each dendrogram, three clusters have been identified for each hydrological period: D1 D2 M1, O1 E1, and D3 D4 D5 D6 D7 E2 for low and mid discharge periods; while D1 O1, D2 M1, and D3 D4 D5 D6 D7 E1 E2 for high discharge period. The greatest differences among groups are in the high discharge hydrological period, where the southern headwater sampling locations are split in two groups,

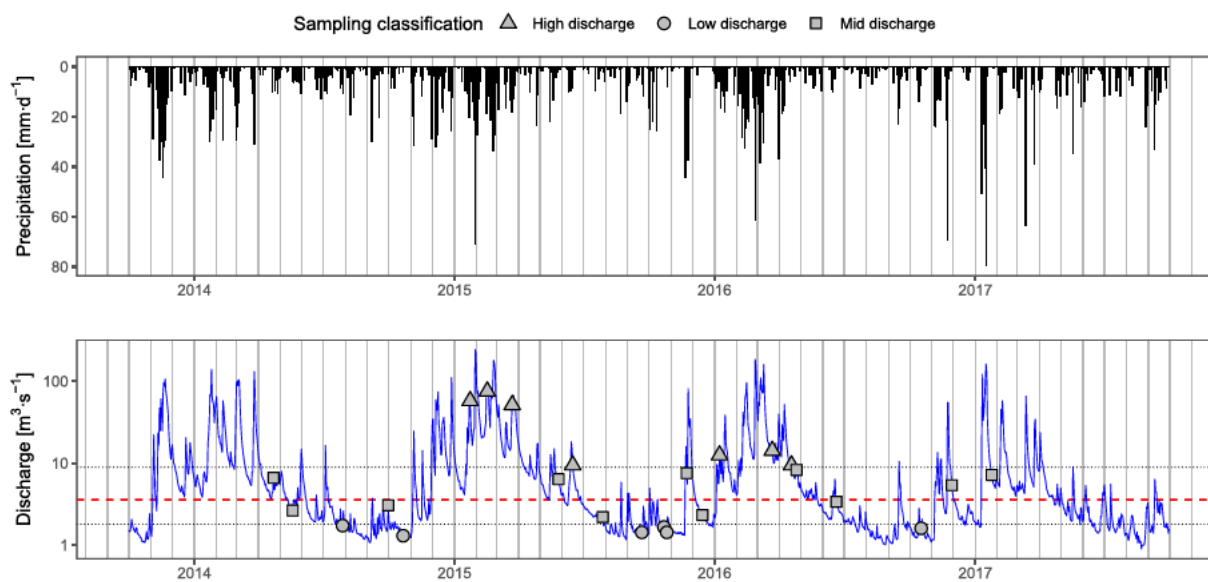


Fig. 3. Daily accumulated precipitation and mean discharge time series at the outlet of the catchment (Altzola gauging station). Vertical axis in precipitation plot is in reverse order, while in the discharge plot it is presented in the logarithmic scale. The horizontal lines in the discharge plot represent the median (dashed line), 1st and 3rd quartiles (25th and 75th percentiles, respectively) used to classify the sampling campaigns into low discharge (triangles), mid discharge (squares), and high discharge (circles). Vertical black lines indicate the starting point of three flood events considered in the present study.

**Table 2**

Pearson correlation test performed on the log-transformed dataset from the punctual sampling for all sampling locations ( $n = 175$ ). Significance of the correlation is displayed through **bold** ( $p < 0.01$ ), *italics* ( $0.01 < p < 0.05$ ), straight ( $p > 0.05$ ).

	pH	TDS <sub>field</sub>	EC <sub>field</sub>	Ca <sup>2+</sup>	Mg <sup>2+</sup>	K <sup>+</sup>	Na <sup>+</sup>	Alkalinity	SO <sub>4</sub> <sup>2-</sup>	Cl	DOC	NO <sub>3</sub>	P-PO <sub>4</sub> <sup>3-</sup>
pH	1.00												
TDS <sub>field</sub>	<b>0.25</b>	1.00											
EC <sub>field</sub>	<b>0.20</b>	<b>1.00</b>	1.00										
Ca <sup>2+</sup>	<b>0.22</b>	<b>0.89</b>	<b>0.90</b>	1.00									
Mg <sup>2+</sup>	<i>0.14</i>	<b>0.89</b>	<b>0.89</b>	<b>0.82</b>	1.00								
K <sup>+</sup>	0.09	<b>0.81</b>	<b>0.82</b>	<b>0.74</b>	<b>0.69</b>	1.00							
Na <sup>+</sup>	<i>0.18</i>	<b>0.93</b>	<b>0.92</b>	<b>0.70</b>	<b>0.83</b>	<b>0.82</b>	1.00						
Alkalinity	<b>0.24</b>	<b>0.59</b>	<b>0.59</b>	<b>0.82</b>	<b>0.42</b>	<b>0.50</b>	<b>0.33</b>	1.00					
SO <sub>4</sub> <sup>2-</sup>	<i>0.15</i>	<b>0.81</b>	<b>0.81</b>	<b>0.66</b>	<b>0.92</b>	<b>0.72</b>	<b>0.85</b>	<b>0.19</b>	1.00				
Cl	<b>0.21</b>	<b>0.90</b>	<b>0.89</b>	<b>0.65</b>	<b>0.74</b>	<b>0.80</b>	<b>0.97</b>	<b>0.33</b>	<b>0.75</b>	1.00			
DOC	<i>0.14</i>	0.09	<i>0.13</i>	0.07	0.02	<b>0.25</b>	0.08	0.10	0.03	0.12	1.00		
NO <sub>3</sub>	<i>0.15</i>	0.09	0.07	0.07	0.08	<b>0.33</b>	<i>0.16</i>	0.10	0.07	<b>0.20</b>	<i>0.14</i>	1.00	
P-PO <sub>4</sub> <sup>3-</sup>	0.03	0.12	0.12	0.11	0.12	<b>0.42</b>	0.14	<b>0.23</b>	0.00	<b>0.20</b>	<b>0.38</b>	<b>0.66</b>	1.00

and the Ego tributary presents more similar characteristics up and downstream. The lower Ward's distances among sampling locations is found in the high discharge period, suggesting lower differences within the catchment in periods with elevated discharge, indicating that discharge has a strong effect on the saline, organic matter, and nutrient concentrations, though dilution conditions the composition in the streams.

In order to understand which variable has a stronger effect on each sampling location, a Principal Component Analysis (PCA) has been performed using the 10 variables dataset selected for the Pearson correlation matrix. Three components with an eigenvalue over 1 account for 79.4% of the total variance, as shown in Fig. 5. Negative values of the F1 relate to sampling locations with high saline concentrations, where M1 and D2 samples stand out. M1 and D2 cluster together in the three sampling periods, representing a single group in the high discharge period, while grouping with D1 in low and mid discharge periods. It has been previously shown that these sampling locations have low nutrients and organic matter concentration, associated with lower anthropogenic input, while the saline characteristics are similar between M1 and D2 due to the strong influence of SO<sub>4</sub><sup>2-</sup> and Ca<sup>2+</sup> derived from the Mazmela tributary (M1) into this section of the main stream. Among the headwaters in this catchment (D1, M1, O1, and E1) M1 and D1 are the most alike in terms of SO<sub>4</sub><sup>2-</sup> concentration, suggesting that the intrusions of gypsum deposits presented in the southwest part of the catchment (EVE, 1989, Ábalos et al., 2008, Martínez Santos et al., 2015) may be responsible of the relatively high concentration of this anion in this first cluster. Negative values of F2 relate to organic matter and nutrient concentrations, where D3 is strongly influenced together with D5, D7, and E2, to a lesser extent. The D3 D4 D5 D6 D7 E2 cluster seems to be strongly affected by nutrient loadings, specially in low and mid

discharge sampling periods, where the two most impacted sampling locations (D3 and E2) stand over the mid and down part of the catchment (D4 D5 D6 D7 group). It seems that in D3 and E2, even after the implementation of management actions such as the Epele WWTP, there is a strong influence of the anthropogenic input, previously noted in the physicochemistry (Unda Calvo et al., 2017) and microbial communities (Martínez Santos et al., 2018; Unda Calvo et al., 2019b) in sediments, as well as in the ecological status linking water and sediments (Unda Calvo et al., 2020). F3 allows for the discretization between two saline kinds of water, those draining halite (D2), and those draining gypsum (M1) waters. It is also relevant to note the clustering of O1 and E1, which is linked to the lower concentration of salts and nutrients in these two sampling locations.

Considering that the D1 D2 D3 and M1 group of sampling locations present both the highest saline and nutrients concentration, and that the main saline input in this area seems to be the evaporitic and stable flow spring located in Leintz Gatzaga (Iribar and Ábalos, 2011). It is important to see how the relative influence of a constant input such as a spring is affecting the major ionic distribution in the catchment, while the hydrological conditions change through time. Further analysis on the temporal evolution is found in Section 3.2.1 (continuous registries).

### 3.1.5. Geochemical processes and water types

Once known that the anthropogenic influence is mainly noted on the nutrients and organic matter, and that major ion composition is dominated by lithology, an assessment on which are the main geochemical processes governing these inputs is performed. The water composition in the Deba river urban catchment varies from headwaters to the outlet of the catchment receiving waters from different tributaries draining in fluents with different water types and a varying degree of pollution

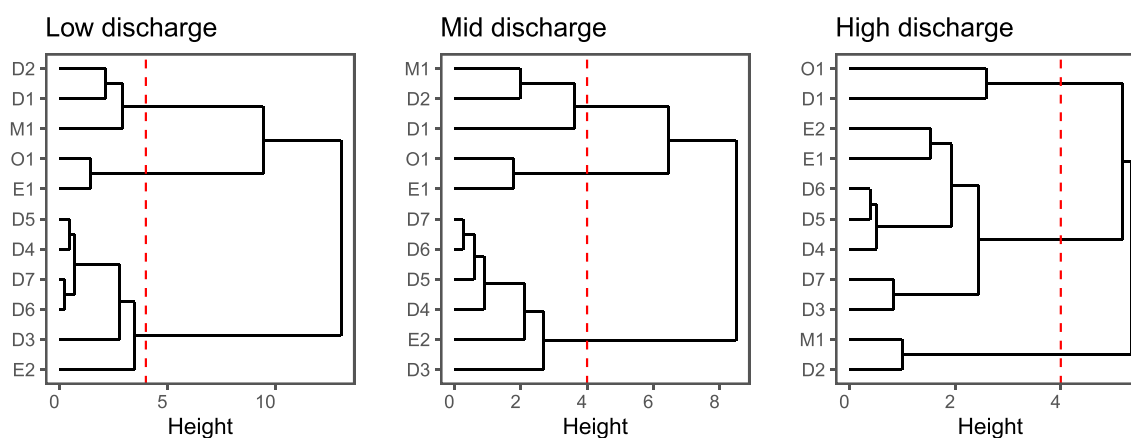


**Fig. 4.** Cluster analysis of the sampling locations in this catchment considering pH, TDS<sub>field</sub>, EC<sub>field</sub>, Ca<sup>2+</sup>, Mg<sup>2+</sup>, Na<sup>+</sup>, Alkalinity, SO<sub>4</sub><sup>2-</sup>, Cl<sup>-</sup>, and P-PO<sub>4</sub><sup>3-</sup> in three different periods. Red dashed line represents a cutting line for three groups.

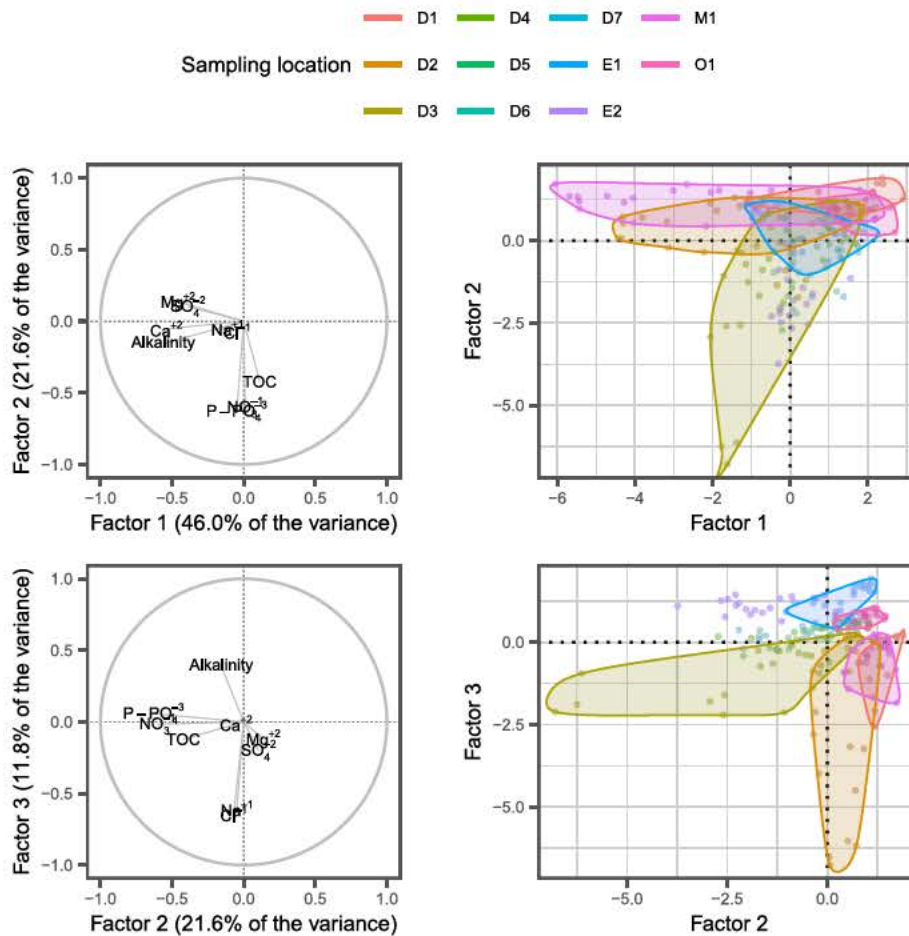


Fig. 5. Principal component analysis (PCA) performed on the major ion, nutrients, and physicochemical variables of the samples. Left plots show the scores of the variables for Factors 1, 2, and 3 (explaining 79.4% of the variance), right plots represent the weights of the factors for each sample included in the analysis. Headwaters (D1, M1, E1, and O1) and D2 are circled to present the major differences.

from treated, partially treated, and untreated industrial and domestic effluents (Martínez Santos et al., 2015, 2018). In order to assess the main geochemical processes given in the catchment, the Gibbs plot (Gibbs, 1970) is used (Fig. S.1), according to which there are three main processes governing the river water composition: crystallization and evaporation, water rock interaction, and precipitation. For this catchment, the Gibbs plot suggests water rock interaction, together with crystallization and evaporation as the main geochemical processes governing major ion composition. The Oñati (O1) and Ego tributaries (E1 and E2) present a low ionic ratio, falling in the left side of the plot, suggesting a strong water rock interaction in this area, related to the low concentration of  $\text{Na}^+$  in comparison with the  $\text{Ca}^{2+}$ , which is probably originated by the carbonate material of the area. The samples from the southeast tributary of Mazmela (M1) cluster around an ionic ratio of 0.25 while presenting a relatively high dissolved solid concentration, specially in the low and mid discharge sampling periods. This suggests a slight tendency towards the crystallization and evaporation zone, but more influenced by the high  $\text{Ca}^{2+}$  concentration, responsible for a lower value of the ionic ratio. The group D1 D2 D3 is pulled to the evaporation crystallization area of the plot which is normally related to seawater intrusion, but in this case is attributed to a saline spring located in Leintz Gatzaga (between D1 and D2, Fig. 1b), which drains water from a deep evaporitic reservoir, as noted by Iribar and Ábalos (2011).

Carbonates is the dominant lithological formation in the catchment, thus an equivalent ratio  $(\text{Ca}^{2+} + \text{Mg}^{2+})/(\text{Alkalinity}) = 1$  indicates that

all  $\text{Ca}^{2+}$  and  $\text{Mg}^{2+}$  come from the dissolution of carbonate materials, while higher values suggest another lithological contribution for  $\text{Ca}^{2+}$  and  $\text{Mg}^{2+}$  than carbonate, i.e. evaporitic rocks (gypsum or epsomite). In this catchment, most of the samples present  $(\text{Ca}^{2+} + \text{Mg}^{2+})/(\text{Alkalinity}) > 1$  (over the dashed line in Fig. 6a), as well as an equivalent ratio  $(\text{SO}_4^{2-})/(\text{HCO}_3^-) > 1$ , while linear relationship between  $\text{Ca}^{2+} + \text{Mg}^{2+}$  and  $\text{SO}_4^{2-} + \text{Alkalinity}$  (Fig. 6b). The greatest deviation from linearity in these two relationships is found for the Mazmela tributary (M1) where there is a relevant amount of  $\text{Ca}^{2+} + \text{Mg}^{2+}$  non balanced by Alkalinity, while a slight predominance of  $\text{SO}_4^{2-} + \text{Alkalinity}$  over those two cations, suggesting a relevant input of  $\text{SO}_4^{2-}$ , confirming the existence of interlayered gypsum deposits (Qin et al., 2018), which are not included in the official map, but has been noted in previous studies (Orive et al., 1989; Iribar and Ábalos, 2011; Martínez Santos et al., 2015).

The Piper Diagram shown in Fig. 7 shows all the water samples collected in the monitoring program distinguished by sampling location and sampling period. It is possible to see that the Deba river and its tributaries samples span over four types of water, presenting higher differences for low and mid discharge sampling periods. Most of the samples are located in the magnesium bicarbonate part of the upper diamond, being dominated mostly by  $\text{Ca}^{2+}$  concentrations, which presents the highest concentrations in the catchment (Table 1). The southwest part of the catchment is associated to the calcium chloride (M1) and the sodium chloride (D1 D2 D3) types of water, while the mid samples are more related to the mixed type. Regarding the anions, the lower right triangle separates the samples in clusters, explaining that M1 is

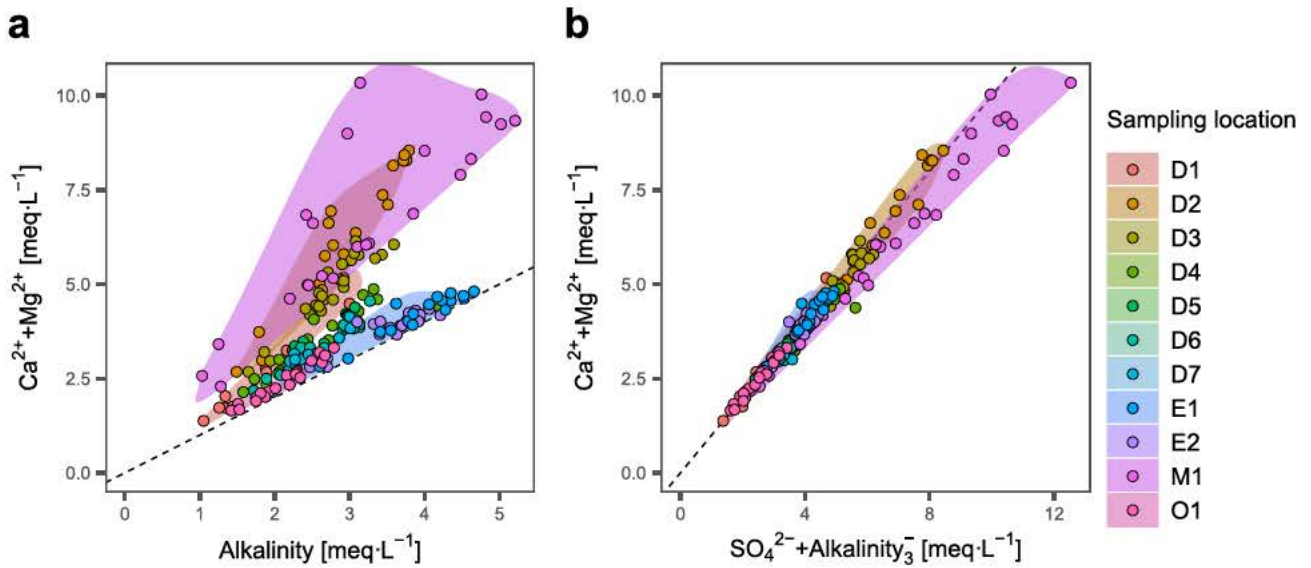


Fig. 6. Ratio scatterplots for punctual sampling results for all sampling locations. Five sampling locations have been circled (D1, D2, M1, O1, and E1) in order to distinguish the different headwaters involved in this catchment, as well as D2. Dashed line represents 1:1 line.

dominated by sulphates supporting the gypsum deposits affecting water chemistry, while D1 and D2 are dragged towards the chloride type, due to the presence of the saline spring. In general, the alkaline earths exceed the alkalis, but the clustering of low and mid discharge samples in D2 and D1 towards the sodium chloride part of the diamond indicates a different behavior of these spots. In D1 D2 M1 it seems that the strong acids (such as  $H_2SO_4$  or  $HCl$ ), related to sulphate and chloride dominate the water chemistry, while in the other sampling locations, the weak acids prevail ( $H_2CO_3$ ).

### 3.2. Water and dissolved solid exports

Two assumptions on the classification of the sampling location have been performed: first, that the results from the punctual sampling campaigns are representative for the daily composition of the river in each location, and that daily mean discharge is enough for the hydrological classification, not taking in consideration previous hydrological conditions (accumulated precipitation, previous discharge, increasing or decreasing part of a flood event...). These assumptions are discussed in

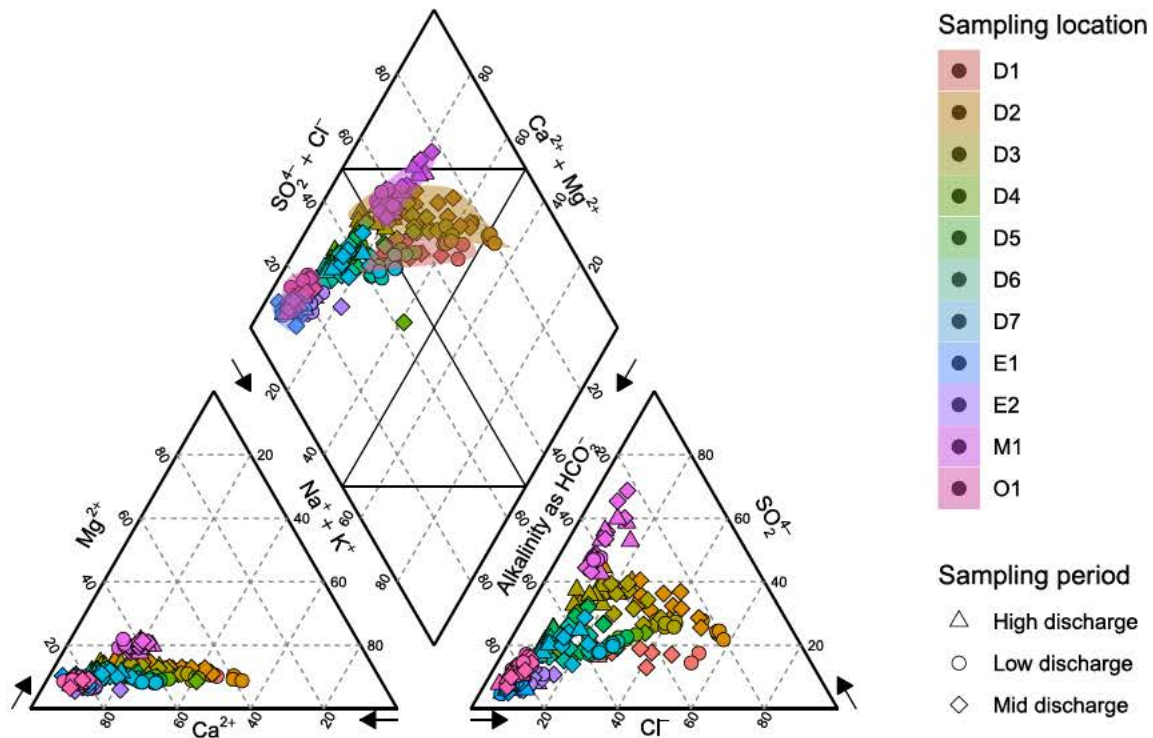


Fig. 7. Piper diagram regarding water classification and geochemical mechanisms governing major ion chemistry at the catchment scale. Each colour represents a single sampling location (the reader is redirected to the web version of the article) while the shape represents the sampling period. Five sampling locations have been circled (D1, D2, M1, O1, and E1) in order to distinguish the different headwaters involved in this catchment, as well as D2 which presents a different kind of water.

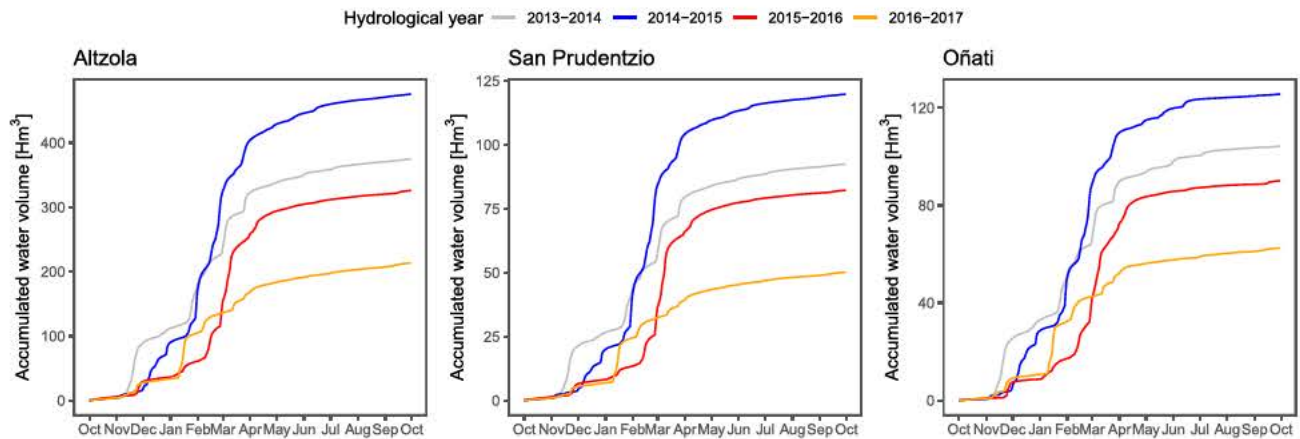


Fig. 8. Accumulated water volume exported in the three gauging stations for the hydrological years (beginning October 1st, ending September 30th) between 2013 and 2017. Each line represents an independent hydrological year.

the following sections. First, regressions are established using punctual data to estimate TDS using EC as proxy in the continuous data registered in three gauging stations (Fig. 1a, b) in Section 3.2.1. Second, the dissolved solid exports are compared taking in consideration different temporal aggregation methods to test the error committed in each time step. And finally, moments of relevant water and dissolved solid loads are evaluated to test which moments are more relevant in terms of TDS or water exports in the present system. All these analyses are performed covering four hydrological years (October 2013–September 2017).

The accumulated time series for water volume (Fig. 8) show that the 2014–2015 was the wettest of the years, followed by 2015–2016 and 2013–2014, while 2016–2017 is the driest period. In general, the lowest discharge periods within these years are between June and November, while relevant flood events contribute to the total water volume exported between December and May. The 2015–2016 and 2016–2017 years overlap in March, before which month the 2015–2016 year was drier, but some flood events increased the total volume discharge. This is true for all three places, where Oñati and San Prudentzio yield comparable water volumes, about half of the total volume discharged on Altzola.

**Table 3** Summary of regressions' estimates (A, B) and coefficients of determination ( $r^2$ ) for each gauging station and corresponding sampling location (between brackets). Four types of regressions are displayed, with estimates shown for best fit: linear, potential, exponential, and logarithmic, along with the formulation. All regressions are fit using EC in  $\mu\text{s}\cdot\text{cm}^{-1}$  and concentrations in  $\text{mg}\cdot\text{L}^{-1}$ , except alkalinity ( $\text{meq}\cdot\text{L}^{-1}$ ). All regressions are significant ( $p < 0.01$ ). Only samples with all variables measured were taken in consideration ( $n$  = number of samples).

Element	Linear		Potential		Logarithmic		$r^2$
	[Element] = A·EC + B		[Element] = A·EC <sup>B</sup>		[Element] = A·ln(EC) + B		
	A	B	A	B	A	B	
<b>Altzola (n = 20)</b>							
TDS <sub>field</sub> ~EC <sub>field</sub>	0.5209	4.7026	–	–	–	–	1.00
EC <sub>field</sub> ~EC <sub>lab</sub>	0.9686	36.647	–	–	–	–	0.98
Ca <sup>2+</sup> ~EC <sub>lab</sub>	35.785	154.81	–	–	–	–	0.96
Mg <sup>2+</sup> ~EC <sub>lab</sub>	–	–	–	–	3.7524	17.5	0.93
Na <sup>+</sup> ~EC <sub>lab</sub>	–	–	0.00005	2.1135	–	–	0.98
K <sup>+</sup> ~EC <sub>lab</sub>	–	–	0.00003	1.8696	–	–	0.88
Alkalinity~EC <sub>lab</sub>	–	–	–	–	1.4177	5.864	0.89
SO <sub>4</sub> <sup>2-</sup> ~EC <sub>lab</sub>	0.0992	0.9197	–	–	–	–	0.81
Cl <sup>-</sup> ~EC <sub>lab</sub>	0.00004	2.2131	–	–	–	–	0.95
<b>San Prudentzio (n = 23)</b>							
TDS <sub>field</sub> ~EC <sub>field</sub>	0.5305	1.876	–	–	–	–	1.00
EC <sub>field</sub> ~EC <sub>lab</sub>	0.9855	30.624	–	–	–	–	1.00
Ca <sup>2+</sup> ~EC <sub>lab</sub>	–	–	–	–	42.389	195.79	0.96
Mg <sup>2+</sup> ~EC <sub>lab</sub>	–	–	–	–	5.1368	23.926	0.82
Na <sup>+</sup> ~EC <sub>lab</sub>	–	–	0.0001	1.9335	–	–	0.99
K <sup>+</sup> ~EC <sub>lab</sub>	–	–	0.00008	1.697	–	–	0.90
Alkalinity~EC <sub>lab</sub>	–	–	–	–	1.2367	5.3158	0.90
SO <sub>4</sub> <sup>2-</sup> ~EC <sub>lab</sub>	–	–	–	–	63.217	307.89	0.84
Cl <sup>-</sup> ~EC <sub>lab</sub>	–	–	0.00006	2.1204	–	–	0.97
<b>Oñati (n = 22)</b>							
TDS <sub>field</sub> ~EC <sub>field</sub>	0.5114	4.5188	–	–	–	–	0.97
EC <sub>field</sub> ~EC <sub>lab</sub>	0.9498	31.938	–	–	–	–	0.91
Ca <sup>2+</sup> ~EC <sub>lab</sub>	–	–	–	–	41.221	181.52	0.91
Mg <sup>2+</sup> ~EC <sub>lab</sub>	–	–	0.0026	1.2632	–	–	0.91
Na <sup>+</sup> ~EC <sub>lab</sub>	0.012	1.3761	–	–	–	–	0.83
K <sup>+</sup> ~EC <sub>lab</sub>	–	–	0.0019	1.1537	–	–	0.46
Alkalinity~EC <sub>lab</sub>	–	–	–	–	1.8526	8.02	0.90
SO <sub>4</sub> <sup>2-</sup> ~EC <sub>lab</sub>	0.1127	11.769	–	–	–	–	0.73
Cl <sup>-</sup> ~EC <sub>lab</sub>	0.0231	0.4847	–	–	–	–	0.41

### 3.2.1. Continuous registries

The monitoring program set up in this catchment contains sampling locations close to the three gauging stations, all of them located within 5 km of the punctual spot: Altzola D6, San Prudentzio D3, and Oñati O1. Due to their proximity and the lack of relevant contributions regarding water chemistry, it has been assumed that the EC in the gauging stations ( $EC_{station}$ ) is a proxy for TDS and major ion composition in those locations. This assumption has been tested through linear regression between EC measurements in laboratory ( $EC_{lab}$ ) and the  $EC_{field}$  measured in punctual sampling locations at the time of sampling, as well as evaluating the regressions between  $TDS_{field}$  and  $EC_{field}$ . In addition, as  $TDS_{field}$  and major ion composition are strongly and very significantly correlated (Table 2) it has been possible, following a similar approach to those of Benettin and van Breukelen (2017), to establish regressions between each element and  $EC_{lab}$  which may be used to deconvolute the  $EC_{station}$  signal into its constituents. Table 3 summarizes these regressions between laboratory and field measurements for each sampling location and its respective gauging station, and Fig. 9 shows the scatterplots for those regressions, as well as the 95% prediction intervals (PI). Most of the samples lay within the PI, and the punctual  $EC_{field}$  strongly correlates to the daily mean  $EC_{station}$ , (Slope > 0.76,  $r^2 > 0.81$ ,  $p < 0.01$ ), suggesting that these regressions may be used to extrapolate a continuous time series of dissolved solids concentrations, as well as major ion concentrations in the river stream.

The agreement between the  $TDS_{field}$  and  $EC_{field}$  and the good correlation between each sampling location with its associated gauging station, allows for the use of the continuous  $EC_{station}$  as proxy for the estimation of TDS concentration which, in combination with continuous discharge, allows for the estimation of dissolved loadings (Fig. 10). Regarding the dissolved solids in the study period, the temporal trends are similar regarding periods, but the steepness of the curves are softer, especially for the case of San Prudentzio, suggesting a relevant contribution during low flow periods and a lower influence of the flood events on the dissolved solid exportation. In addition, the differences among the years are lower in San Prudentzio, suggesting a more stable load along the year. Regarding the ranges of the loadings, those of San Prudentzio are almost double the ones in Oñati, about a third of those measured in Altzola, suggesting a strong dependence of this area of the catchment on the loadings exported out of the basin.

As expected, the combination of high frequency data from the gauging locations with the periodic sampling results have shown significant regressions between  $EC_{lab}$  and ionic concentrations. The obtained regression coefficients pose an opportunity for developing a time dependent analysis of the major ion loadings from the Deba river to the estuary, where the riverine end member input is important when assessing the estuarine dynamics and the land pollutant estimation (Tueros et al., 2008). For this purpose, the continuous measurement of  $EC_{station}$  in the Altzola gauging station is key, as it collects the waters for most part of the catchment. The knowledge of a continuous dissolved solids concentration and major ion chemical composition is of interest for biogeochemical modelling focusing in riverine loads to other water bodies (such as lakes, estuaries, or oceans) (Chapra et al., 2012). In addition, it is possible to characterize these loadings in terms of their ionic concentration, as they show strong and significant correlations to  $EC_{lab}$ , the time series are shown in Fig. 11.

### 3.2.2. Dissolved solid loadings

The obtained regressions from the punctual data have allowed us to compute the  $TDS_{station}$  concentration temporal evolution, which is now used to estimate the annual loadings to the estuary of the Deba catchment, using Altzola gauging station as the outlet point. In this study, we have compared three methodologies (Table 4) on the estimation of these loadings for the three gauging stations present in the system, taking into account different temporal steps. Method 1 is based on the mean discharge and mean concentration during all the period, Method 2 accounts for the moments with punctual samplings, while Method 3

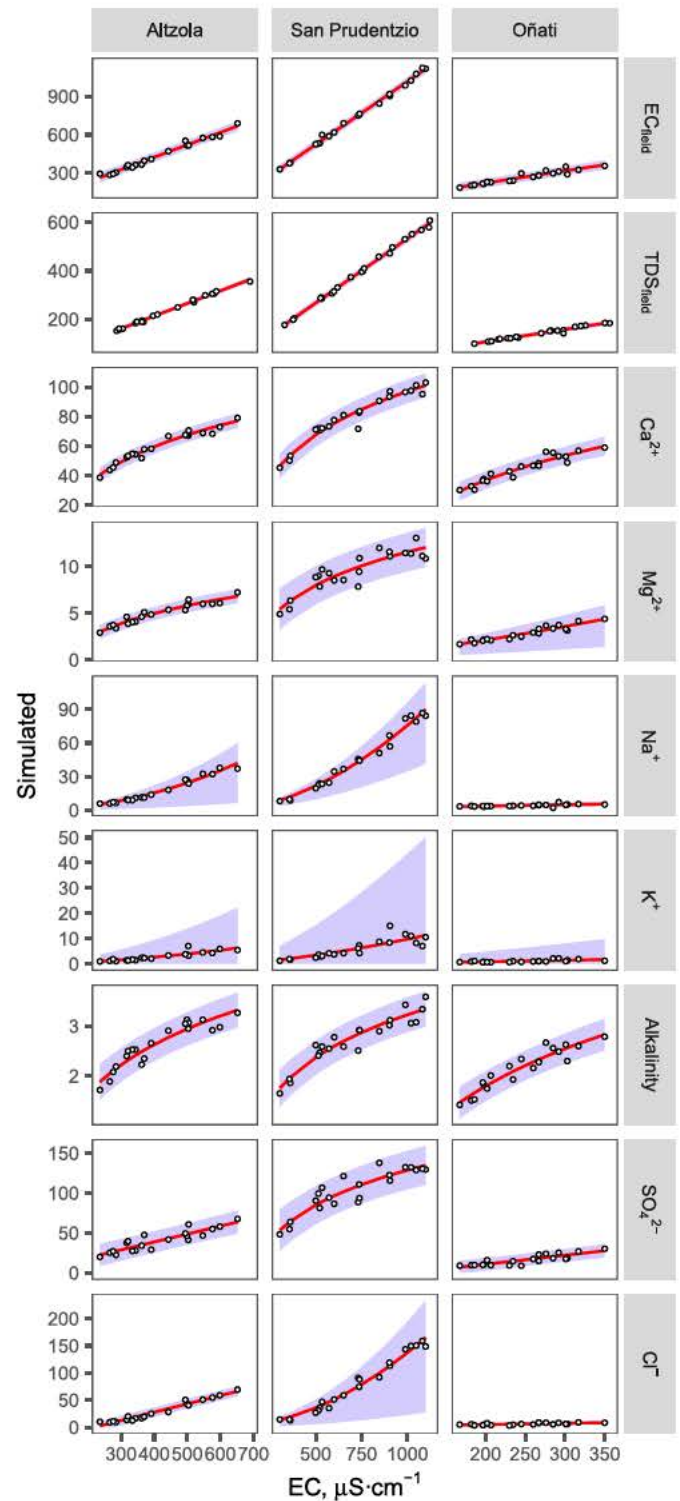


Fig. 9. Scatter plot of ionic concentrations,  $TDS_{field}$  and  $EC_{field}$  vs  $EC_{lab}$  in each sampling location close to its associated gauging station. Points represent punctual samples; red line indicates simple linear regression (estimates and regression evaluation are shown in Table 3), and blue area indicate 95% prediction intervals.

used the integration of the daily mean discharge ( $Q_{station}$ ) and  $TDS_{station}$  concentration finding that, as finer the temporal resolution is, the lower the load becomes, suggesting that methods 1 and 2 overestimates the annual dissolved solid input. This insight highlights the advantages of establishing a continuous monitoring program with high frequency

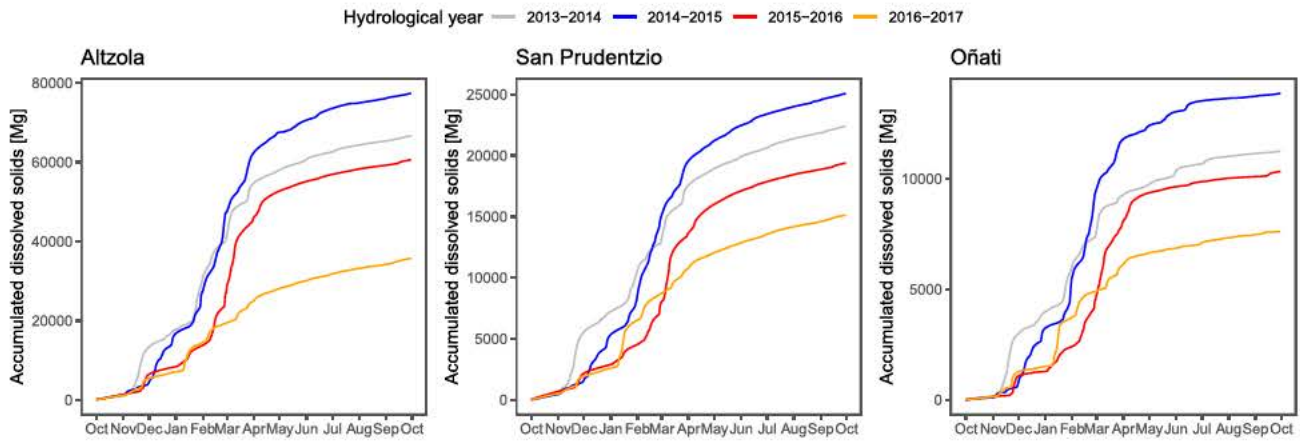


Fig. 10. Accumulated dissolved solids exported in the three gauging stations for the hydrological years (beginning October 1st, ending September 30th) between 2013 and 2017. Each line represents an independent hydrological year.

registries, which can improve this assessment through periodic monitoring program. Specially in systems such as the Deba river, where differences in river discharge span over two orders of magnitude

between low flow period and high flow period. In such system like Deba, with a fast response to the precipitation, flood events are common (García García et al., 2019) and floods have been studied as moments of

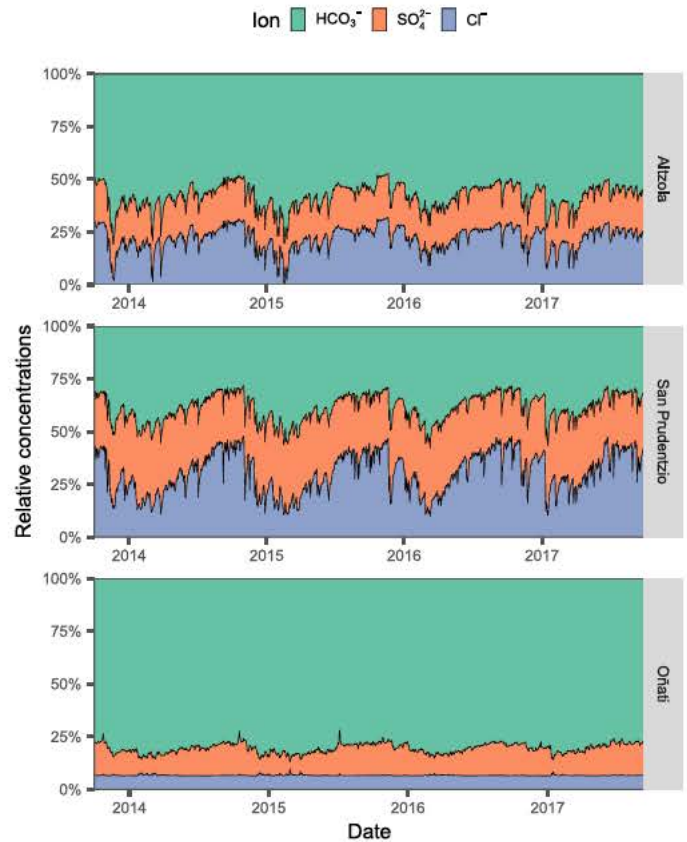
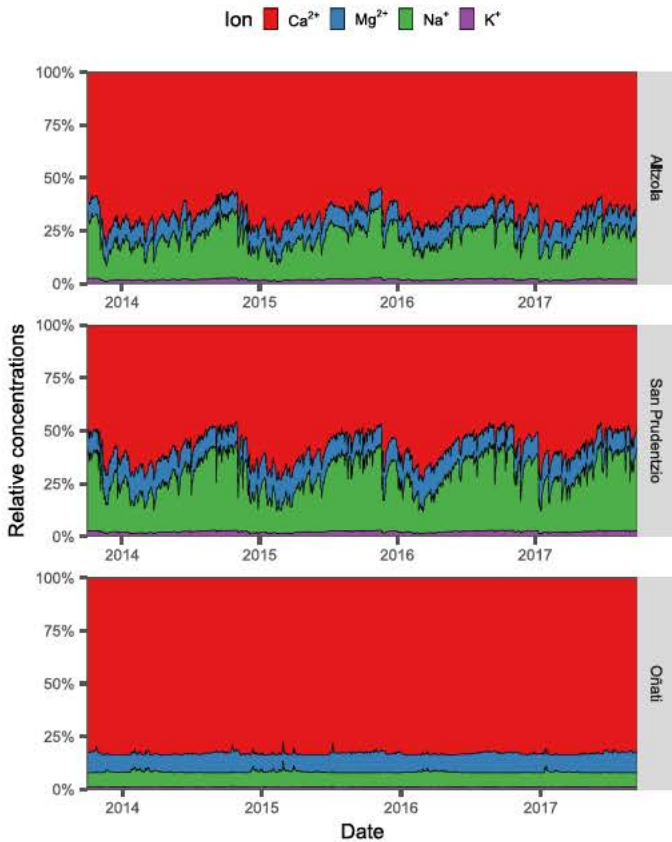
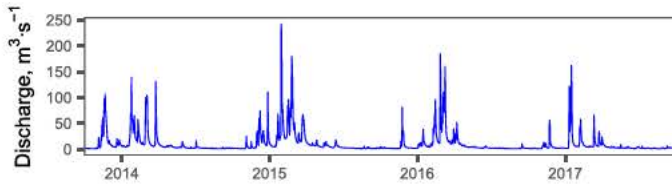


Fig. 11. Major ion relative concentration time series for all three gauging stations. Areas represent the relative proportion of a ionic concentration respect the total cation ( $Z^+ / \sum Z^+$ ) or anion ( $Z^- / \sum Z^-$ ) concentration, respectively. Percentages are calculated using equivalent concentrations.

**Table 4**

Summary of Total Dissolved Solid exports in three sampling locations in the Deba river catchment. All units are expressed as  $\text{Mg} \cdot \text{y}^{-1}$ , computed as indicated in the Equation column.  $L_{\text{annual}}$  is mean annual load,  $k$  represents the unit conversion factor,  $\overline{\text{TDS}}$  represents the Total Dissolved Solid concentration ( $\overline{\text{TDS}}$  is the average concentration among all sampling campaigns,  $\text{TDS}$  represents instant concentration, and  $\text{TDS}'$  the obtained through linear regression with Electrical Conductivity, all expressed in  $\text{mg} \cdot \text{L}^{-1}$ ),  $Q$  represents discharge (similar differences as for  $\text{TDS}$ , expressed in  $\text{m}^3 \cdot \text{s}^{-1}$ ),  $\Delta t$  is the time span (measured in days), and  $dt$  represents the daily increment used for the integration.

	Equation	D3 San Prudentzio	O1 Oñati	D6 Altzola
Method 1	$L_{\text{annual}} = k \cdot \overline{\text{TDS}} \cdot \overline{Q}$	36,572	16,414	92,384
Method 2	$L_{\text{annual}} = \sum L_{i+1} \cdot k \cdot \sum \left( \frac{\text{TDS}_i + \text{TDS}_{i+1}}{2} \cdot \frac{Q_i + Q_{i+1}}{2} \cdot \Delta t \right)$	26,940	13,395	75,579
Method 3	$L_{\text{annual}} = f(Q, \text{TDS}) = k \cdot \int_0^{\text{year}} Q(t) \cdot \text{TDS}'(t) \cdot dt$	15,888	8383	46,435

wash up of the catchment, becoming relevant events for matter transport from land to the ocean. The effect of these events on the major ion composition has not assessed in urban catchments such as the one in this study, where the anthropogenic activity could lead to the deposition of salts in the soil which are washed out during flood events. In this moment, we pose the following question: when are the moments where the exportation of dissolved solids is most relevant? To answer this question, we use the continuous registries in the Altzola gauging station, in combination with the regressions obtained (Table 3) to compute a time series of dissolved solids and compare which is the error committed when using lower temporal resolution data.

Table 5 presents the TDS annual loadings ( $L_{\text{annual}}$ ) using Method 3 from Table 4, and different temporal aggregations, and we compare them with those loadings obtained using only the punctual sampling locations. Note that only two full hydrological years are covered by the sampling program and are included in the analysis. In general, the finer the frequency, the lower the error committed, but no relevant errors (>15%) are found for 1 h or 1 day aggregation, which could justify the use of the aggregated time series and the consideration of the punctual sampling results as representative of the mean daily concentration. Monthly aggregation implies a higher degree of error (>21%) reaching, in some hydrologic years an overestimation of 50%. Considering only the average discharge and TDS concentration between pairs of sampling campaigns (Method 2 in table) yielded higher uncertainties, with an overestimation of the load in 2014–2015 hydrologic year, and an underestimation of the load in 2015–2016. This suggests that, for the Deba river catchment, the response time of the catchment is fast ( $\leq 1$  day), creating a need of continuous registries to quantify the exports of dissolved loads with an acceptable error. In this system, the use of punctual data as the daily average comprises greater uncertainty in period with higher discharge, but this error is under 15%.

**Table 5**

Summary of Total Dissolved Solid exports in the Altzola gauging station using different aggregation methods for the continuous registries, and the sampling campaign data from sampling location D6. Errors among aggregation methods are shown for each hydrologic year covered in the present study. Only 2014–2015 and 2015–2016 hydrologic years are shown in the Samplings column, due to those are the only ones fully covered by the monitoring program.

Total dissolved solids (TDS) loadings ( $\text{Mg} \cdot \text{y}^{-1}$ )					
Hydrologic year	10 min	1 h	1 day	1 month	Samplings
2013–2014	65,888	66,541	69,183	79,862	–
2014–2015	69,337	69,824	78,034	94,258	153,763
2015–2016	58,059	58,197	63,476	74,909	37,551
2016–2017	33,401	33,586	36,236	50,636	–

Error (%) = $(L - L_{10\text{min}}) / L_{10\text{min}}$					
Hydrologic year	10 min	1 h	1 day	1 month	Samplings
2013–2014	–	1.0%	5.0%	21.2%	–
2014–2015	–	0.7%	12.5%	35.9%	121.8%
2015–2016	–	0.2%	9.3%	29.0%	35.3%
2016–2017	–	0.6%	8.5%	51.6%	–

### 3.2.3. Seasonality

Considering 1 day as the minimum threshold for dissolved matter exportation in the present catchment, an analysis for the study period has shown which are the moments of relevance for the total dissolved matter exportation and the saline concentration. Fig. 12 contains the time series for discharge and the difference from the relative contribution between water volume and dissolved loadings. In such figure, it is possible to see that, depending on the increasing or decreasing branch of the flood event, the relative input of water volume or dissolved solids differs. The monthly evolution shows a seasonality occurring between February and March every year, as well as November, December and April some years, where the relative contribution of water prevails over the exportation of dissolved loadings, which is commonly higher in November 2015, and January 2017. This is associated to a higher number of flood events in these periods, where diluted meteoric water decreases saline concentration while increasing water volume exports. Focusing on the daily time series (Fig. 12b), the greater contribution of dissolved loads occurs at the end of those flood events, specially when the flood event occurs after a period of maintained low discharge (focus on November 2015 or January 2017). Such insight suggests that, in the present system, the greatest peaks of discharge are loaded with low concentrations of salts, decreasing the salinity in the estuary in periods of flood events (Ladouche et al., 2001), but the response of the soil and groundwater is fast, implying a rapid recovery of dissolved concentration, thus increasing the loadings in the decreasing part of the flood events.

The analysis of the hysteresis is relevant to understand the origin of water and the transport phenomena occurring in a system. With the aim of evaluating the dilution effect in this catchment, Fig. 13 presents the daily and monthly  $\text{EC}_{\text{station}}$  and discharge for the Altzola gauging station for the study period. In general, a linear relationship may be found for all years, with a slight clockwise pattern found for 2015–2016 year. Such pattern suggests that the response of the catchment to flood events is fast and homogeneous, where dilution occurs in all the catchment at the same time, and the water from the furthest part of the catchment reaches the outlet (Altzola gauging station) later than the water close to the station. As this water is already diluted, the lowest concentration in salts (here proxy as EC) is reached at the same time (linear) or after the peak discharge (clockwise). This confirms that the greatest donor of saline concentrations is lithology, and that human impact in this catchment does not have a relevant influence on major ion presence.

### 3.3. Punctual and continuous integration

The physicochemical analysis of water has commonly been performed through monitoring programs based on punctual samplings (e.g. Şener et al., 2017; Unda Calvo et al., 2019a). However, limitations on instantaneous and intermittent water sampling use for load estimation has been highlighted before (Cassidy and Jordan, 2011), as temporal variability in daily or seasonal processes is not always fully captured by punctual sampling. Extrapolation of punctual measurements to

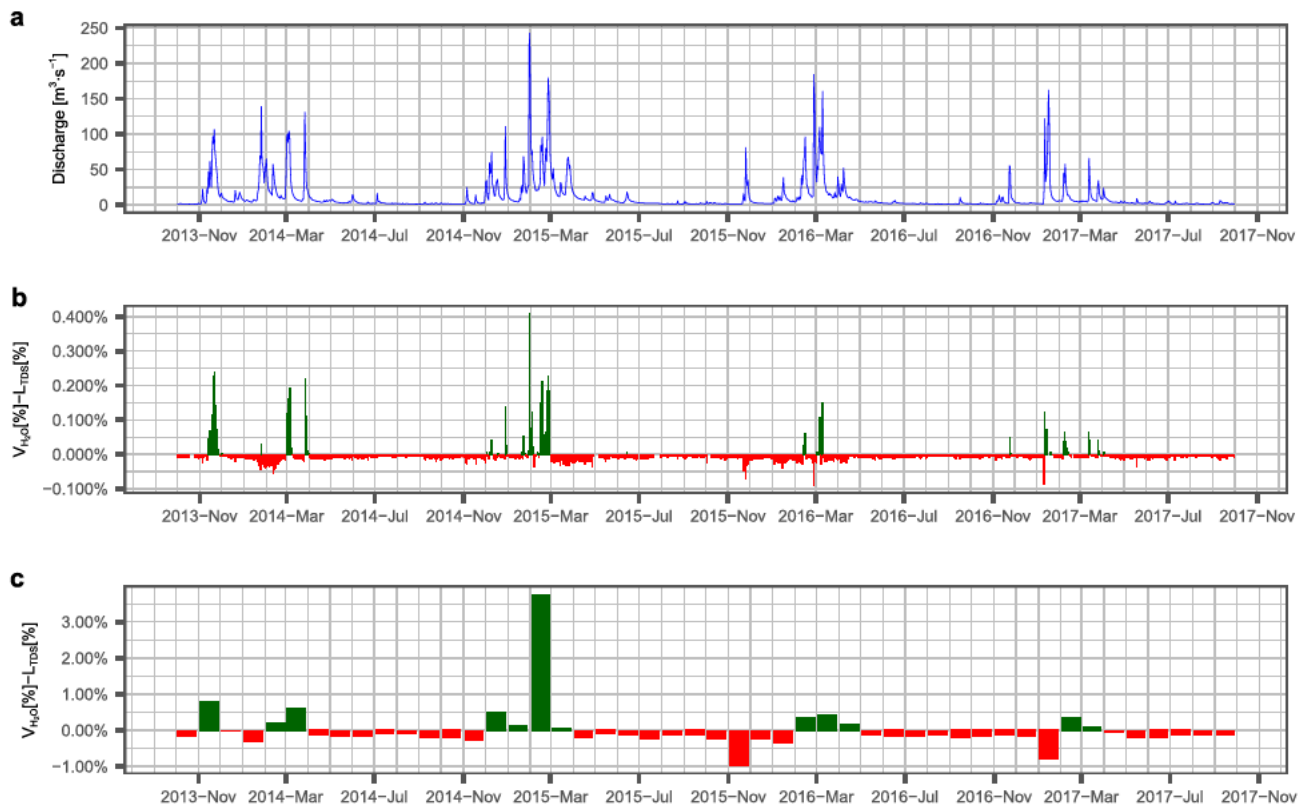


Fig. 12. Temporal evolution of a) discharge, b) daily and c) monthly difference in the relative contribution of water volume ( $V_{H_2O}$ ) and dissolved load ( $L_{TDS}$ ) to the total exports in the study period.

continuous time series has long been performed, specially for the analysis of physical erosion and the quantification of sediment export yields (e.g. Peraza Castro et al., 2015). However, such relationships are less common regarding dissolved solid concentrations, which allows the assessment of changes in salinity, conditioning which industrial or agricultural uses that water is plausible for (Ball et al., 2020), the characterization of the riverine endmember in estuarine dynamics (Pontes Franco et al., 2019), or the understanding of other physico-chemical processes given in the water matrix (oxygen dissolution, flocculation,  $CO_2$  exchange, carbonate precipitation, nitrate consumption...), of interest for matter transport in biogeochemical cycles (Dessert et al., 2020; Ponnou Delaffon et al., 2020). Here, the comparison among different frequencies used for dissolved saline loadings calculations (Table 5) has shown that the variability in this system, linked mainly to hydrological changes, needs at least a daily assessment for long term loads. Then, even though the role of in situ sensors for ecological monitoring in rivers is being recognised more recently (Rode et al., 2016), the combination of both punctual and continuous methodologies has been needed for the present assessment, as continuous measurements of individual ions has not been possible.

As major ions, nutrients, and DOC have not been continuously monitored, the understanding of dissolved loading origin has been accomplished through the results of the punctual sampling. Here, the spatial distribution of the punctual samplings has allowed the understanding of which are the main geochemical processes, where are located, and which is their temporal evolution in the long term. Even though it is an urban catchment which has long been considered as polluted due to industrial and urban effluents (Martínez Santos et al., 2015; Unda Calvo et al., 2020), anthropogenic activity exerts a greater impact on nutrients and metals than in major ion composition. This is seen as D2 concentrations on all major ions is dominant in mostly all ions, suggesting that the saline spring input is the main responsible for the major composition of the main channel (Figs. 2, 8). Such influence over major

ion composition is noted both in the punctual sampling campaigns as well as in the continuous integration, as the regressions for most of the ions are non linear where, depending on the saline concentration, the ionic composition varies.

In summary, the two methodologies applied in the present analysis have given necessary and complementary information the present assessment: the spatial evaluation of main processes governing water chemistry, and its temporal evolution. The combination of both methodologies has recently allowed to evidence, for some elements, nycthemeral cycles due to biogeochemical processes (Ponnou Delaffon et al., 2020). This combination has also been used to quantify dissolved loadings in urban environments (Viviano et al., 2014), and nutrient loadings in agricultural catchments (e.g. Ferrant et al., 2013), but in the present study it has allowed the estimation of saline loadings, as well as their characterization among its major constituents. Alternatives to this combined method include the use of composite samples (e.g. Merchán et al., 2019) which give a single average daily value before computing daily loadings, or the use of frequent sampling for estimation of temporal variations (e.g. El Najjar et al., 2019). The fit of regressions with punctual data, and its application on continuous registries, allows not only for the approximation of the daily load, but also the establishment of a prediction interval (i.e. uncertainty assessment) in these loadings, as well as the quantification of the error committed when using temporal aggregations. The quantification of the uncertainty and the error committed in the temporal aggregation is a valuable information for stakeholders regarding the establishment of future monitoring programs and one way of optimizing the monitoring activities (Singh et al., 2004).

#### 4. Conclusion

The major ion composition of the urban Deba river varies from head waters to the outlet of the catchment while receiving effluents from

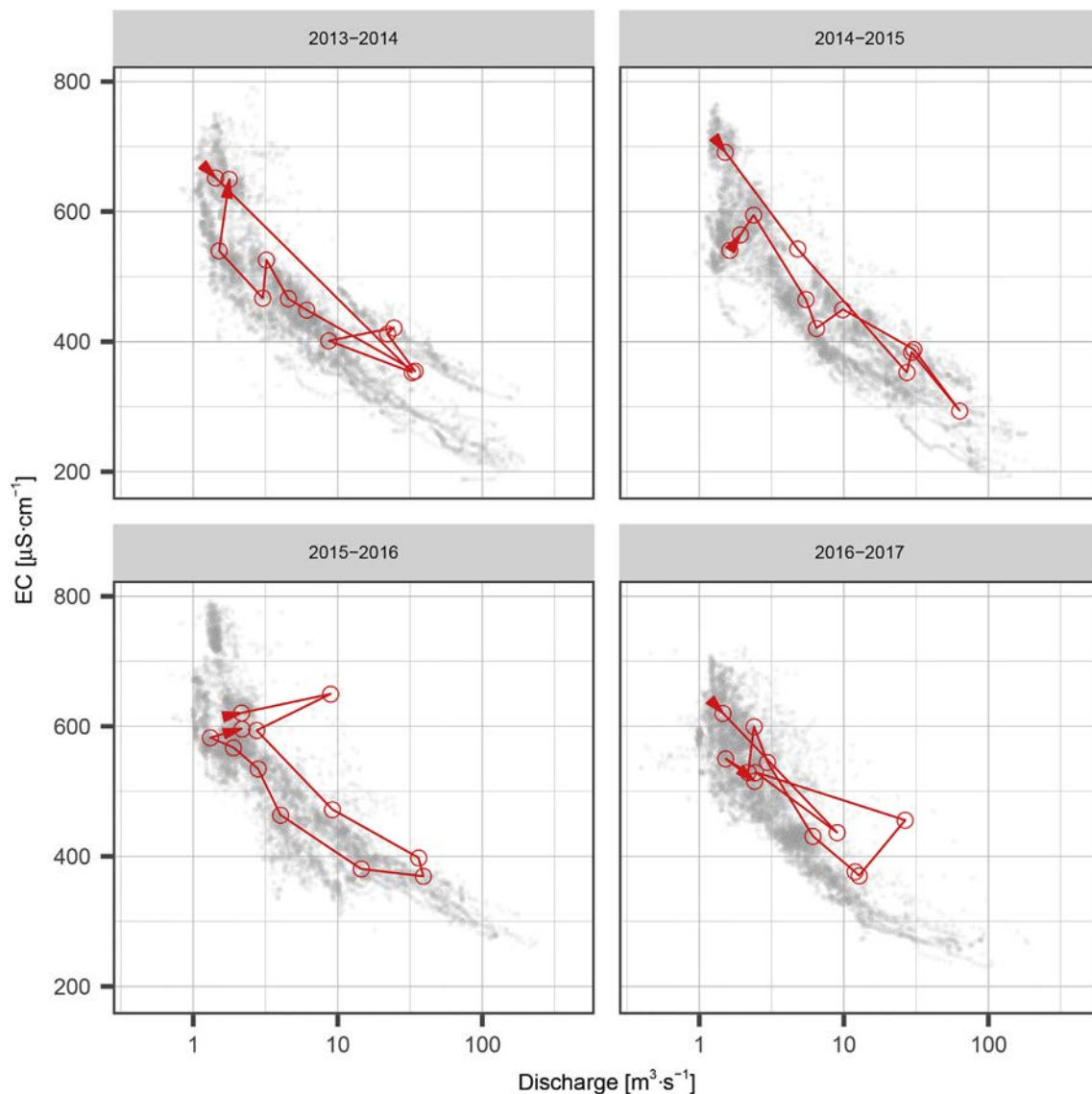


**Fig. 13.** Monthly hysteresis in Altzola gauging station for each hydrologic year considered in the study. Grey points represent every daily record, while red lines and arrows indicate monthly averages.

tributaries, urban and industrial treated and untreated wastewaters. Punctual data has shown that the major ion composition is mainly affected by the natural geochemical processes given in the catchment, which are related to water rock interaction and crystallization evaporation, while nutrients remain related to treated and partially treated wastewater. The major source of  $\text{Na}^+$  and  $\text{Cl}^-$  in the river is associated to evaporitic spring between D1 and D2, while  $\text{Ca}^{2+}$  and  $\text{SO}_4^{2-}$  are derived from gypsum deposits in M1, all these ions located in the southwest part of the catchment. The southeast, mid and down part of the catchment drains mainly sedimentary carbonate rocks, but the outlet characteristics are mostly affected by the southwest part of the catchment. Only  $\text{K}^+$  presents a different spatial pattern in the catchment, suggesting that anthropogenic input has a stronger effect on this major ion, and nutrients ( $\text{NO}_3^-$ ,  $\text{P}$ ,  $\text{PO}_4^{3-}$ ), as peak concentrations are found downstream of the WWTP effluents. The inclusion of high frequency registries has allowed for the extrapolation of punctual measures to continuous time series, which allow for the assessment of annual exports, as well as the evaluation of the error committed when considering low resolution data on the assessment of such annual loadings. Continuous registries have allowed the identification of moments with higher influence of dissolved solids: the last part of the flood

events, where the runoff is low and sub surface and groundwater flow are dominant. In this system, errors under 15% are found when considering 1 day measurements, which carries high cost for punctual sampling. Such cost may be avoided by combining punctual sampling results with continuous registries, as has been done in the present analysis. Further research is needed on using these continuous data on the assessment of estuarine dynamics, as well as exploring the applicability of these continuous time series on the evaluation of modelling for the estimation of the continuum land ocean matter exports, specially in the terms of Global Change.

Supplementary data to this article can be found online at <https://doi.org/10.1016/j.scitotenv.2020.138644>.

#### CRedit authorship contribution statement

**Juan Luis Lechuga-Crespo:** Conceptualization, Methodology, Validation, Formal analysis, Investigation, Data curation, Writing original draft, Writing review & editing, Visualization. **Estilita Ruiz-Romera:** Conceptualization, Methodology, Validation, Formal analysis, Investigation, Resources, Data curation, Writing original draft, Writing review & editing, Supervision, Project administration, Funding acquisition.

**Jean-Luc Probst:** Conceptualization, Validation, Investigation, Writing review & editing, Visualization. **Jessica Unda-Calvo:** Data curation, Formal analysis, Writing original draft. **Zaira Carolina Cuervo-Fuentes:** Conceptualization, Validation, Formal analysis, Investigation, Writing original draft. **José Miguel Sánchez-Pérez:** Conceptualization, Validation, Investigation, Writing review & editing, Supervision.

## Declaration of competing interest

The authors declare that they have no known competing financial interests or personal relationships that could have appeared to influence the work reported in this paper.

## Acknowledgments

The authors wish to thank the Ministry of Economy and Competitiveness (CTM2014 55270 R), the Consolidated Group of Hydrogeology and Environment (IT1029 16, Basque Government), the University of the Basque Country (UPV/EHU), and the Institut National Polytechnique de Toulouse (INPT) for supporting this research.

## References

- Ábalos, B., Alkorta, A., Iríbar, V., 2008. Geological and isotopic constraints on the structure of the Bilbao anticlinorium (Basque–Cantabrian basin, North Spain). *J. Struct. Geol.* 30 (11), 1354–1367. <https://doi.org/10.1016/j.jsg.2008.07.008>.
- Álvarez-Vázquez, M.A., Prego, R., Ospina-Alvarez, N., Caetano, M., Bernárdez, P., Doval, M., et al., 2016. Anthropogenic changes in the fluxes to estuaries: wastewater discharges compared with river loads in small rias. *Estuar. Coast. Shelf Sci.* 179, 112–123. <https://doi.org/10.1016/j.ecss.2015.08.022>.
- Anderson, O.R., 2016. The role of heterotrophic microbial communities in estuarine C budgets and the biogeochemical C cycle with implications for global warming: research opportunities and challenges. *J. Eukaryot. Microbiol.* 63 (3), 394–409. <https://doi.org/10.1111/jeu.12279>.
- Ball, L.B., Bedrosian, P.A., Minsley, B.J., 2020. High-resolution mapping of the freshwater-brine interface using deterministic and Bayesian inversion of airborne electromagnetic data at Paradox Valley, USA. *Hydrogeol. J.* 95 (4), 664. <https://doi.org/10.1007/s10040-019-02102-z>.
- Benettin, P., van Breukelen, B.M., 2017. Decomposing the bulk electrical conductivity of streamflow to recover individual solute concentrations at high frequency. *Environ. Sci. Technol. Lett.* 4 (12), 518–522. <https://doi.org/10.1021/acs.estlett.7b00472>.
- Cañedo-Argüelles, M., Kefford, B.J., Piscart, C., Prat, N., Schäfer, R.B., Schulz, C.J., 2013. Salinisation of rivers: an urgent ecological issue. *Environ. Pollut. (Barking, Essex: 1987)* 173, 157–167. <https://doi.org/10.1016/j.envpol.2012.10.011>.
- Cassidy, R., Jordan, P., 2011. Limitations of instantaneous water quality sampling in surface-water catchments: comparison with near-continuous phosphorus time-series data. *J. Hydrol.* 405 (1–2), 182–193. <https://doi.org/10.1016/j.jhydrol.2011.05.020>.
- Chapra, S.C., Dove, A., Warren, G.J., 2012. Long-term trends of Great Lakes major ion chemistry. *J. Great Lakes Res.* 38 (3), 550–560. <https://doi.org/10.1016/j.jglr.2012.06.010>.
- Dessert, C., Clergue, C., Rousteau, A., Crispi, O., Benedetti, M.F., 2020. Atmospheric contribution to cations cycling in highly weathered catchment, Guadeloupe (Lesser Antilles). *Chem. Geol.* 531, 119354. <https://doi.org/10.1016/j.chemgeo.2019.119354>.
- EEA, 2012. CORINE Land Cover (20). Retrieved from: <https://land.copernicus.eu/pan-european/corine-land-cover/clc-2012?tab=download>.
- El Najjar, P., Kassouf, A., Probst, A., Probst, J.L., Ouaini, N., Daou, C., El Azzi, D., 2019. High-frequency monitoring of surface water quality at the outlet of the Ibrahim River (Lebanon): a multivariate assessment. *Ecol. Indic.* 104, 13–23. <https://doi.org/10.1016/j.ecolind.2019.04.061>.
- Elzhov, T.V., Mullen, K.M., Spiess, A.N., Bolker, B., 2016. minpack.lm: R interface to the Levenberg-Marquardt nonlinear least-squares algorithm found in MINPACK, plus support for bounds. R package version 1.2-1. <https://CRAN.R-project.org/package=minpack.lm>.
- EVE-Ente Vasco de la Energía, 1989. *Mapa geológico del País Vasco*. 63I, 63III, 88-I, 88-III.
- FAO, IIASA, ISRIC, ISS-CAS, JRC, 2012. *Harmonized World Soil Database. Version 1.2*. FAO, Rome, Italy and IIASA, Luxenburg, Austria.
- Ferrant, S., Laplanche, C., Durbe, G., Probst, A., Dugast, P., Durand, P., et al., 2013. Continuous measurement of nitrate concentration in a highly event-responsive agricultural catchment in south-west of France: is the gain of information useful? *Hydrol. Process.* 27 (12), 1751–1763. <https://doi.org/10.1002/hyp.9324>.
- García-García, Jon, Ruiz-Romera, Estilita, Martínez-Santos, Miren, Antigüedad, Iñaki, 2019. Temporal variability of metallic properties during flood events in the Deba River urban catchment (Basque Country, Northern Spain) after the introduction of sewage treatment systems. *Environ. Earth Sci.* 78 (1), 402. <https://doi.org/10.1007/s12665-018-8014-1>.
- Ghanem, Samar Khairy, 2018. The relationship between population and the environment and its impact on sustainable development in Egypt using a multi-equation model. *Environ. Dev. Sustain.* 20 (1), 305–342. <https://doi.org/10.1007/s10668-016-9882-8>.
- Gibbs, R., 1970. *Mechanisms controlling world water chemistry*. Science 170.
- Graham, L.P., Hagemann, S., Jaun, S., Beniston, M., 2007. On interpreting hydrological change from regional climate models. *Clim. Chang.* 81 (S1), 97–122. <https://doi.org/10.1007/s10584-006-9217-0>.
- Herbert, Ellen R., Boon, Paul, Burgin, Amy J., Neubauer, Scott C., Franklin, Rima B., Ardón, Marcelo, et al., 2015. A global perspective on wetland salinization: ecological consequences of a growing threat to freshwater wetlands. *Ecosphere* 6 (10), 206. <https://doi.org/10.1890/ES14-00534.1>.
- Iribar, V., Ábalos, B., 2011. The geochemical and isotopic record of evaporite recycling in spas and salterns of the Basque Cantabrian basin, Spain. *Appl. Geochem.* 26 (8), 1315–1329. <https://doi.org/10.1016/j.apgeochem.2011.05.005>.
- Kaushal, Sujay S., Duan, Shuiwang, Doody, Thomas R., Haq, Shahan, Smith, Rose M., Newcomer, Johnson, Tamara, A., et al., 2017. Human-accelerated weathering increases salinization, major ions, and alkalization in fresh water across land use. *Appl. Geochem.* 83, 121–135. <https://doi.org/10.1016/j.apgeochem.2017.02.006>.
- Khatri, Nitasha, Tyagi, Sanjiv, 2015. Influences of natural and anthropogenic factors on surface and groundwater quality in rural and urban areas. *Front. Life Sci.* 8 (1), 23–39. <https://doi.org/10.1080/21553769.2014.933716>.
- Ladouche, B., Probst, A., Viville, D., Idir, S., Baqué, D., Loubet, M., et al., 2001. *Hydrograph separation using isotopic, chemical and hydrological approaches (Strengbach catchment, France)*. *J. Hydrol.* 242, 255–274.
- Launay, Marie A., Dittmer, Ulrich, Steinmetz, Heidrun, 2016. Organic micropollutants discharged by combined sewer overflows - characterisation of pollutant sources and stormwater-related processes. *Water Res.* 104, 82–92. <https://doi.org/10.1016/j.watres.2016.07.068>.
- Martínez-Santos, Miren, Probst, Anne, García-García, Jon, Ruiz-Romera, Estilita, 2015. Influence of anthropogenic inputs and a high-magnitude flood event on metal contamination pattern in surface bottom sediments from the Deba River urban catchment. *Sci. Total Environ.* 514, 10–25. <https://doi.org/10.1016/j.scitotenv.2015.01.078>.
- Martínez-Santos, Miren, Lanzén, Anders, Unda-Calvo, Jessica, Martín, Iker, Garbisu, Carlos, Ruiz-Romera, Estilita, 2018. Treated and untreated wastewater effluents alter river sediment bacterial communities involved in nitrogen and sulphur cycling. *Sci. Total Environ.* 633, 1051–1061. <https://doi.org/10.1016/j.scitotenv.2018.03.229>.
- Mendizabal, M., Sepúlveda, J., Torp, P., 2014. Climate change impacts on flood events and its consequences on human in Deba River. *Int. J. Environ. Res.* 8 (1), 221–230.
- Merchán, D., Luquin, E., Hernández-García, I., Campo-Bescós, M.A., Giménez, R., Casali, J., Del Valle de Lersundi, J., 2019. Dissolved solids and suspended sediment dynamics from five small agricultural watersheds in Navarre, Spain: a 10-year study. *Catena* 173, 114–130. <https://doi.org/10.1016/j.catena.2018.10.013>.
- Merchán, D., Sanz, L., Alfaro, A., Pérez, I., Goñi, M., Solsona, F., et al., 2020. Irrigation implementation promotes increases in salinity and nitrate concentration in the lower reaches of the Cidacos River (Navarre, Spain). *Sci. Total Environ.* 706, 135701. <https://doi.org/10.1016/j.scitotenv.2019.135701>.
- Montagna, P., Palmer, T.A., Polack, J., 2013. *Hydrological Changes and Estuarine Dynamics*. 1st ed. 8. Springer Briefs in Environmental Science, Springer-Verlag New York. <https://doi.org/10.1007/978-1-4614-5833-3>.
- Nielsen, D.L., Brock, M.A., Rees, G.N., Baldwin, D.S., 2003. Effects of increasing salinity on freshwater ecosystems in Australia. *Aust. J. Bot.* 51 (6), 655. <https://doi.org/10.1071/BT02115>.
- Orive, E., Basaguren, A., de Bikuña, B., Cacho, M., 1989. *A comparative study of water mineralization and nutrient status in the main water courses of Biscay (Basque Country)*. *Water Res.* 23 (6), 705–710.
- Peraza-Castro, M., Ruiz-Romera, E., Montoya-Armenta, L.H., Sánchez-Pérez, J.M., Sauvage, S., 2015. Evaluation of hydrology, suspended sediment and Nickel loads in a small watershed in Basque Country (Northern Spain) using eco-hydrological SWAT model. *Ann. Limnol. Int. J. Lim.* 51 (1), 59–70. <https://doi.org/10.1051/limn/2015006>.
- Ponnou-Delaffon, V., Probst, A., Payre-Suc, V., Granouillac, F., Ferrant, S., Perrin, A.S., Probst, J.L., 2020. Long and short-term trends of stream hydrochemistry and high frequency surveys as indicators of the influence of climate change, agricultural practices and inner processes (Aurade agricultural catchment, SW France). *Ecol. Indic.*, 110 <https://doi.org/10.1016/j.ecolind.2019.105894>.
- Pontes Franco, T., Neves, L., Mitrano, Araújo, Francisco Gerson, 2019. Better with more or less salt? The association of fish assemblages in coastal lagoons with different salinity ranges. *Hydrobiologia* 828 (1), 83–100. <https://doi.org/10.1007/s10750-018-3804-8>.
- Qin, T., Yang, P., Groves, C., Chen, F., Xie, G., Zhan, Z., 2018. Natural and anthropogenic factors affecting geochemistry of the Jialing and Yangtze Rivers in urban Chongqing, SW China. *Appl. Geochem.* 98, 448–458. <https://doi.org/10.1016/j.apgeochem.2018.10.009>.
- R Core Team, 2019. *R: A language and environment for statistical computing*. R Foundation for Statistical Computing, Vienna, Austria Available online at: <https://www.R-project.org/>.
- Rode, M., Wade, A.J., Cohen, M.J., Hensley, R.T., Bowes, M.J., Kirchner, J.W., et al., 2016. Sensors in the stream: the high-frequency wave of the present. *Environ. Sci. Technol.* 50 (19), 10297–10307. <https://doi.org/10.1021/acs.est.6b02155>.
- Şener, Ş., Şener, E., Davraz, A., 2017. Evaluation of water quality using water quality index (WQI) method and GIS in Aksu River (SW-Turkey). *Sci. Total Environ.* 584–585, 131–144. <https://doi.org/10.1016/j.scitotenv.2017.01.102>.
- Singh, K.P., Malik, A., Mohan, D., Sinha, S., 2004. Multivariate statistical techniques for the evaluation of spatial and temporal variations in water quality of Gomti River (India)—a case study. *Water Res.* 38 (18), 3980–3992. <https://doi.org/10.1016/j.watres.2004.06.011>.
- Spiess, A.N., 2018. *Propagate: propagation of uncertainty*. R package version 1.0-6. <https://CRAN.R-project.org/package=propagate>.

- Tueros, I., Rodríguez, J.G., Borja, A., Solaun, O., Valencia, V., Millán, E., 2008. Dissolved metal background levels in marine waters, for the assessment of the physico-chemical status, within the European Water Framework Directive. *Sci. Total Environ.* 407 (1), 40–52. <https://doi.org/10.1016/j.scitotenv.2008.08.026>.
- Unda-Calvo, J., Martínez-Santos, M., Ruiz-Romera, E., 2017. Chemical and physiological metal bioaccessibility assessment in surface bottom sediments from the Deba River urban catchment: harmonization of PBET, TCLP and BCR sequential extraction methods. *Ecotoxicol. Environ. Saf.* 138, 260–270. <https://doi.org/10.1016/j.ecoenv.2016.12.029>.
- Unda-Calvo, J., Ruiz-Romera, E., Fdez-Ortiz de Vallejuelo, S., Martínez-Santos, M., Gredilla, A., 2019a. Evaluating the role of particle size on urban environmental geochemistry of metals in surface sediments. *Sci. Total Environ.* 646, 121–133. <https://doi.org/10.1016/j.scitotenv.2018.07.172>.
- Unda-Calvo, J., Martínez-Santos, M., Ruiz-Romera, E., Lechuga-Crespo, J.L., 2019b. Implications of denitrification in the ecological status of an urban river using enzymatic activities in sediments as an indicator. *J. Environ. Sci. (China)* 75, 255–268. <https://doi.org/10.1016/j.jes.2018.03.037>.
- Unda-Calvo, J., Ruiz-Romera, E., Martínez-Santos, M., Vidal, M., Antigüedad, I., 2020. Multivariate statistical analyses for water and sediment quality index development: a study of susceptibility in an urban river. *Sci. Total Environ.* 711, 135026. <https://doi.org/10.1016/j.scitotenv.2019.135026>.
- URA. 2019. Red de seguimiento del estado biológico de los ríos de la Comunidad Autónoma del País Vasco. Informe de resultados. Campaña 2018. Available online at. <https://uragentzia.euskadi.eus>.
- Vitousek, P.M., Aber, J.D., Howarth, R.W., Likens, G.E., Matson, P.A., ... Schindler, D.W., 1997. Human alteration of the global nitrogen cycle: sources and consequences. *Ecol. Appl.* 7 (3), 737–750. [https://doi.org/10.1890/1051-0761\(1997\)007\[0737:HAOTGN\]2.0.CO;2](https://doi.org/10.1890/1051-0761(1997)007[0737:HAOTGN]2.0.CO;2).
- Vitousek, P.M., Naylor, R., Crews, T., David, M.B., Drinkwater, L.E., Holland, E., et al., 2009. Agriculture. Nutrient imbalances in agricultural development. *Science* (New York, N.Y.) 324 (5934), 1519–1520. <https://doi.org/10.1126/science.1170261>.
- Viviano, G., Salerno, F., Manfredi, E.C., Polesello, S., Valsecchi, S., Tartari, G., 2014. Surrogate measures for providing high frequency estimates of total phosphorus concentrations in urban watersheds. *Water Res.* 64, 265–277. <https://doi.org/10.1016/j.watres.2014.07.009>.
- Vörösmarty, C.J., McIntyre, P.B., Gessner, M.O., Dudgeon, D., Prusevich, A., Green, P., et al., 2010. Global threats to human water security and river biodiversity. *Nature* 467 (7315), 555–561. <https://doi.org/10.1038/nature09440>.
- Wickham, Hadley, 2016. *ggplot 2: elegant graphics for data analysis*. Springer-Verlag, New York Available online at. <https://ggplot2.tidyverse.org>.